

Accepted to *The Astrophysical Journal*

Dust Extinction Curves and Ly α Forest Flux Deficits for Use in Modeling GRB Afterglows and All Other Extragalactic Point Sources

Daniel E. Reichart^{1,2,3}

ABSTRACT

Since gamma-ray burst afterglows were first detected in 1997, the relativistic fireball model has emerged as the leading theoretical explanation of the afterglows. In this paper, we present a very general, Bayesian inference formalism with which this, or any other, afterglow model can be tested, and with which the parameter values of acceptable models can be constrained, given the available photometry. However, before model comparison or parameter estimation can be attempted, one must also consider the physical processes that affect the afterglow as it propagates along the line of sight from the burst source to the observer. Namely, how does extinction by dust, both in the host galaxy and in our galaxy, and absorption by the Ly α forest and by H I in the host galaxy, change the intrinsic spectrum of the afterglow? Consequently, we also present in this paper a very general, eight-parameter dust extinction curve model, and a two-parameter model of the Ly α forest flux deficit versus redshift distribution. Using fitted extinction curves from Milky Way and Magellanic Cloud lines of sight, and measurements of Ly α forest flux deficits from quasar absorption line systems, we construct a Bayesian prior probability distribution that weights this additional, but necessary, parameter space such that the volume of the solution space is reduced significantly, *a priori*. Finally, we discuss the broad applicability of these results to the modeling of light from all other extragalactic point sources, such as Type Ia supernovae.

Subject headings: dust, extinction — galaxies: ISM — gamma-rays: bursts — stars: formation — quasars: absorption lines — ultraviolet: ISM

¹Department of Astronomy and Astrophysics, University of Chicago, 5640 South Ellis Avenue, Chicago, IL 60637

²Department of Astronomy, California Institute of Technology, Mail Code 105-24, 1201 East California Boulevard, Pasadena, CA 91125

³Hubble Fellow

1. Introduction

Optical afterglows have been detected for at least twelve gamma-ray bursts (GRBs); underlying galaxies have been detected for at least seven of these. Underlying galaxies have been detected by high-resolution imaging with HST [Sahu et al. 1997; Fruchter et al. 1999a (GRB 970228); Fruchter et al. 1999b (GRB 970508); Kulkarni et al. 1998 (GRB 971214); Fruchter 1999b, private communication (GRB 980329); Bloom et al. 1999a; Fruchter et al. 1999c (GRB 990123); Fruchter 1999c, private communication (GRB 990712)], by medium-resolution, ground-based imaging [e.g., Djorgovski et al. 1998a,b (GRB 980613)], by detecting emission lines at afterglow locations [e.g., Djorgovski et al. 1998c (GRB 980613); Djorgovski et al. 1998d (980703)], and by sampling afterglow light curves until an asymptotic value is approached [e.g., Bloom et al. 1998 (GRB 980703)]. However, this last method is not always reliable, as Bloom et al. (1999b) have shown that a brightening supernova component to an afterglow light curve can be misinterpreted as being due to an underlying galaxy if the light curve is not sufficiently well-sampled at late times (see also Hjorth et al. 1999). Lamb (1999) has shown that underlying galaxies that have been confirmed to be coincident with their afterglows by high-resolution, *HST* imaging are host galaxies to a high degree of certainty; however, $\approx 10 - 15\%$ of the remaining underlying galaxies are probably chance coincidences. Consequently, at least six of these underlying galaxies are host galaxies, and the remaining one or two underlying galaxies are very likely to be host galaxies as well.

Since many, if not all, of the long bursts with detected optical afterglows are associated with host galaxies, these afterglows are likely to be extinguished by dust in their host galaxies (Reichart 1997), as well as by dust in our galaxy, and absorbed by H I in their host galaxies, as well as by the Ly α forest (Fruchter 1999a). These physical processes affect - in some cases, probably significantly - the observed spectra of afterglows from the infrared (IR) through the ultraviolet (UV). For example, Lamb & Reichart (2000a,b) suggest that some of the ≈ 13 bursts with securely-detected X-ray afterglows, but without securely-detected optical afterglows, might be explained by large amounts of extinction by dust in their host galaxies, probably from the immediate vicinities of these bursts if they are indeed associated with star-forming regions (see Lamb & Reichart 2000a for a discussion of the evidence in favor of this association), or by absorption by the Ly α forest if these bursts occur at very high redshifts ($z \gtrsim 5$).

Since the majority of afterglow observations are made at optical and near-infrared wavelengths, the effects of these physical processes on the observed spectra cannot be ignored, particularly since these spectra have been redshifted. Indeed, these effects must be carefully modeled if intrinsic spectra are to be recovered. This is the primary purpose of this paper. The secondary purpose of this paper is to present a very general, Bayesian inference formalism with which afterglow models can be tested, and with which the parameter values of acceptable models can be constrained, given the available photometry. We begin with this in §2. Also in §2, we develop and present a formalism for the construction of Bayesian prior probability distributions from multi-dimensional data sets, which we draw on extensively in §4 and §5. In §3, we present an eight-parameter dust

extinction curve model, based on the work of Fitzpatrick & Massa (1988) and Cardelli, Clayton, & Mathis (1989). In §4, we construct a prior that weights this additional parameter space such that the volume of the solution space is reduced significantly, *a priori*, using fitted extinction curves from Milky Way and Magellanic Cloud lines of sight. In §5, we present a two-parameter model of the Ly α forest flux deficit versus redshift distribution, and we construct an analogous prior using Ly α forest flux deficit measurements from quasar absorption line systems. In §6, we present a wide variety of extinguished and absorbed spectral flux distributions, using these models. In §7, we draw conclusions, including a discussion of the broad applicability of these results to the modeling of light from all other extragalactic point sources.

2. Statistical Methodology

In §2.1, we present a very general, Bayesian inference formalism with which afterglow models (and any other model for that matter) can be tested, and with which the parameter values of acceptable models can be constrained, given the available photometry. In §2.2, we develop and present a formalism for the construction of Bayesian prior probability distributions from multi-dimensional data sets, which we draw on extensively in §4 and §5. For a deeper discussion of Bayesian inference, we refer the reader to an excellent review by Loredo (1992).

2.1. Bayesian Inference

2.1.1. Bayes' Theorem

Bayes' theorem states:

$$p(H|DI) = \frac{p(H|I)p(D|HI)}{p(D|I)}, \quad (1)$$

where H is the hypothesis, or model, being considered, D is the data, and I is any available prior information. Hence, Bayes' theorem states that the probability of a given hypothesis, $p(H|DI)$, given the data and any available prior information, is proportional to the product of the probability of the hypothesis, $p(H|I)$, given the prior information, and the probability of the data, $p(D|HI)$, given the hypothesis and the prior information. The quantity $p(H|DI)$ is called the posterior probability distribution, the quantity $p(H|I)$ is called the prior probability distribution, and the quantity $p(D|HI)$ - sometimes denoted $\mathcal{L}(H)$ - is called the likelihood function.

The quantity $p(D|I)$ normalizes the posterior. Let the hypothesis, or model, H , be described by a set of parameters θ . Then, Bayes' theorem reads:

$$p(\theta|DI) = \frac{p(\theta|I)p(D|\theta I)}{p(D|I)}. \quad (2)$$

Normalization demands that

$$\int_{\theta} p(\theta|DI)d\theta = 1; \quad (3)$$

hence, $p(D|I)$ is given by

$$p(D|I) = \int_{\theta} p(\theta|I)p(D|\theta I)d\theta. \quad (4)$$

Consequently, given a prior (see §2.1.2) and a likelihood function (see §2.1.3), a normalized posterior may be computed.

2.1.2. The Prior

Let $\{\theta\}$ denote the region over which the parameters θ are integrated in Equations (3) and (4). The prior, $p(\theta|I)$, describes how any available pre-existing information constrains the values of the parameters θ , or equivalently, how any available pre-existing information weights the parameter space $\{\theta\}$, and consequently, reduces the volume of the solution space, *a priori*.

If no prior information is available, one usually takes the prior to be flat within a region $\{\theta_{phys}\} \subset \{\theta\}$ where the values of the parameters θ are considered to be physically plausible; the prior is taken to be zero everywhere else:

$$p(\theta|I) = \begin{cases} (\int_{\theta_{phys}} d\theta)^{-1} & (\theta \in \{\theta_{phys}\}) \\ 0 & (\theta \notin \{\theta_{phys}\}) \end{cases}; \quad (5)$$

here, the volume integral normalizes the prior.⁴ The flat prior weights, *a priori*, all physically-plausible solutions equally, and gives no weight to physically-imausible solutions.

As an example, consider the case of a two-parameter model, where the parameters, x and y , are physically unrelated. In this case, the prior factorizes:

$$p(x, y|I) = p(x|I)p(y|I). \quad (6)$$

Furthermore, suppose that prior information states that the possible values of x are normally distributed with a mean of a and a standard deviation of b , but that no prior information is available on the value of y , other than that values of $y < y_l$ and $y > y_u$ are considered physically implausible. Then, the prior for the parameter x , given the prior information a and b , is given by

$$p(x|a, b) = G(x, a, b), \quad (7)$$

where $G(x, a, b)$ is a normalized Gaussian distribution, given by

$$G(x, a, b) = \frac{1}{\sqrt{2\pi}b} \exp \left[-\frac{1}{2} \left(\frac{x-a}{b} \right)^2 \right], \quad (8)$$

⁴Here, we consider only linearly flat priors; however, logarithmically flat priors are also used, particularly when $\{\theta_{phys}\}$ spans orders of magnitude.

and the prior for the parameter y , given the prior information y_l and y_u , is given by

$$p(y|y_l, y_u) = F(y, y_l, y_u), \quad (9)$$

where $F(y, y_l, y_u)$ is a flat prior, given by

$$F(y, y_l, y_u) = \begin{cases} (y_u - y_l)^{-1} & (y_l < y < y_u) \\ 0 & (\text{otherwise}) \end{cases}. \quad (10)$$

We make extensive use of Gaussian and flat priors in this paper, particularly in §2.2. We present specific priors for parameters that describe the effects of extinction and absorption along the lines of sight to bursts in §4 and §5, respectively.

2.1.3. The Likelihood Function

The likelihood function, $p(D|\theta I)$, describes how any available data constrain the values of the parameters θ , or equivalently, how any available data weight the parameter space $\{\theta\}$, and consequently, reduce the volume of the solution space. Consequently, the posterior, $p(\theta|DI)$, which is proportional to the product of the prior and the likelihood function, describes how prior information and data jointly constrain the values of the parameters θ , or equivalently, how prior information and data jointly weight the parameter space $\{\theta\}$, and consequently, jointly reduce the volume of the solution space.

We now consider the form of the likelihood function for an unspecified afterglow model (and for any other spectral and temporal model for that matter). Let $F_\nu(\nu, t; \theta)$ be the model's prediction for the spectral flux of an afterglow; $F_\nu(\nu, t; \theta)$ is a function of frequency of observation, ν , time of observation, t , and the model parameters, θ , which should include parameters that describe the effects of extinction and absorption along the line of sight. Given N measured spectral fluxes, the likelihood function is given by

$$p(D|\theta I) = \prod_{n=1}^N G_n[F_\nu(\nu_n, t_n; \theta), F_{\nu,n}, \sigma_{F_{\nu,n}}], \quad (11)$$

where $F_{\nu,n}$ is the n th measured spectral flux, $\sigma_{F_{\nu,n}}$ is the measured $1-\sigma$ uncertainty associated with this spectral flux, and $G_n[F_\nu(\nu_n, t_n; \theta), F_{\nu,n}, \sigma_{F_{\nu,n}}]$ is a normalized Gaussian distribution, given by Equation (8).

2.1.4. Model Comparison

Model comparison allows one to asses the relative probability of two or more models; consequently, this procedure may be used to reject non-viable models. Here, we consider the case

of only two models; however, one can easily generalize the following procedure to the case of multiple models.

Consider two models, H_θ and H_ϕ , that are described by two sets of parameters, θ and ϕ , respectively. The relative probability of model H_θ to model H_ϕ is called the odds ratio, and is given by

$$O_{\theta\phi} = \frac{\int_\theta p(\theta|DI)d\theta}{\int_\phi p(\phi|DI)d\phi} \quad (12)$$

$$= \frac{\int_\theta p(\theta|I)p(D|\theta I)d\theta}{\int_\phi p(\phi|I)p(D|\phi I)d\phi}. \quad (13)$$

Normalization demands that

$$\int_\theta p(\theta|DI)d\theta + \int_\phi p(\phi|DI)d\phi = 1; \quad (14)$$

hence, given only models H_θ and H_ϕ , the probability in favor of model H_θ is

$$\int_\theta p(\theta|DI)d\theta = \frac{O_{\theta\phi}}{1 + O_{\theta\phi}}, \quad (15)$$

and the probability in favor of model H_ϕ is

$$\int_\phi p(\phi|DI)d\phi = \frac{1}{1 + O_{\theta\phi}}. \quad (16)$$

2.1.5. Parameter Estimation

Parameter estimation allows one to constrain parameter values of acceptable models. This procedure has two parts: marginalization and the determination of credible regions.

Consider a single model, H , that is described by two sets of parameters: interesting parameters, θ , whose values one wishes to constrain, and uninteresting parameters, ϕ , whose values one does not need to constrain. Then, Bayes' theorem reads:

$$p(\theta\phi|DI) = \frac{p(\theta\phi|I)p(D|\theta\phi I)}{p(D|I)}. \quad (17)$$

The posterior of the interesting parameters, $p(\theta|DI)$, is given by integrating the full posterior, $p(\theta\phi|DI)$, over the uninteresting parameters, ϕ , and by then normalizing the resulting distribution:

$$p(\theta|DI) = \frac{\int_\phi p(\theta\phi|I)p(D|\theta\phi I)d\phi}{\int_{\theta\phi} p(\theta\phi|I)p(D|\theta\phi I)d\theta d\phi}. \quad (18)$$

This procedure is called marginalization.

Credible regions are determined by integrating the posterior from the most probable region of $\{\theta\}$ to the least probable region of $\{\theta\}$ until p % of the distribution has been integrated:

$$\int_{\theta_p} p(\theta|DI)d\theta = \frac{p}{100}, \quad (19)$$

where $\{\theta_p\} \subset \{\theta\}$ such that $p(\theta_1|DI) > p(\theta_2|DI)$ for any $\theta_1 \in \{\theta_p\}$ and for any $\theta_2 \in \{\theta\} - \{\theta_p\}$. The region $\{\theta_p\}$ is called the p % credible region of the parameters θ , or the solution space. Of course, one can imagine many regions - actually an infinite number of regions - that integration over yields p % of the distribution; however, by integrating over the most probable region of $\{\theta\}$, one guarantees that the volume of $\{\theta_p\}$ is minimal, and that $\{\theta_p\}$ is uniquely defined.

2.2. Constructing Priors from Multi-Dimensional Data Sets

In §3, we present an eight-parameter model that describes the effects of extinction by dust along the lines of sight to bursts (and along the lines of sight to all extragalactic point sources for that matter). However, without a prior that weights this parameter space such that the volume of the solution space is reduced significantly, *a priori*, this model has very little predictive power. Fortunately, a considerable amount of prior information - in the form of fitted values for six of these eight parameters from 166 measured Milky Way and Magellanic Cloud extinction curves, and fitted values for one of the two remaining parameters from 79 of these extinction curves - exists; we describe this multi-dimensional data set in §4. In this section, we develop and present a formalism by which priors can be extracted from multi-dimensional data sets; we draw on this formalism extensively in §4 and §5. The extraction of a simply-formulated prior from, for example, the above, large, multi-dimensional data set greatly facilitates the incorporation of this prior information in future afterglow analyses. We begin with a sequence of four illustrative examples in §2.2.1, the last three of which are particularly relevant to our construction of the dust extinction curve prior in §4.

2.2.1. Examples in Three Dimensions and their Generalization

With the first example, we describe the form that the prior should take in the ideal case of one (or more) of the quantities in the data set being fully determined by other quantities in the data set, and of this relation between these quantities being either known or easily determined from the data set. With the second example, we describe the form that the prior should take in the less ideal case of this relation between these quantities existing, but of its existence not being known or easily determined from the data set, although correlations between subsets of these quantities are determinable from the data set. With the third example, we describe the form that the prior should take in the related case of this relation not being determinable from the data set because it involves quantities that are not in the data set, although correlations between the

quantities that are in the data set, or subsets of these quantities, are determinable from the data set. This last example is particularly realistic in that one often deals with physical processes, like dust extinction, that, although understood in general, many of the details of which depend on quantities whose relevance has not even been postulated yet, let alone whose values have been measured. With the final example, we describe the form that the prior should take in the event that data selection effects, either due to instrumental limitations or due to how the sample was selected at a more human level, artificially constrain the values of quantities in the data set. We then discuss our generalization of these examples into a procedure.

Example 1. Consider a three-dimensional data set that consists of measured values of the parameters w , x , and y . Furthermore, suppose that these parameters are related by $y = x + w$, and that w and x are physically-unrelated parameters whose measured values are distributed as the Gaussians $G(w, 0, 0.1)$ and $G(x, 0, 1)$, i.e., as $w = 0 \pm 0.1$ and $x = 0 \pm 1$. Consequently, the measured values of the parameter y should also be distributed as a Gaussian, namely, $G(y, 0, 1.005)$. In this case, the prior that best represents this data set is given by

$$p(w, x, y|I) = G(w, 0, 0.1)G(x, 0, 1)\delta(y - x - w). \quad (20)$$

This prior weights the three-dimensional parameter space, consequently reducing the volume of the solution space to a localized region of a two-dimensional plane, *a priori*.

Example 2. Suppose now that the relation $y = x + w$ exists, but that its existence has not yet been determined. One way to learn of this relation is to plot the data in three dimensions (or to plot the data in two dimensions and use perspective, or different symbols, or different colors, etc., to represent the third dimension). However, this approach is increasingly difficult to implement in increasingly-higher dimensions. Another approach is to probe the data set mathematically. However, without prior knowledge of the form of the relation, let alone knowledge of its existence, this approach also can fail, particularly if the relation is non-linear in form. Consequently, we now consider the form that the prior should take in the event that the relation $y = x + w$ is not known. In this case, one approach is to plot the data two parameters at a time. Having done this, one would immediately notice that the parameters x and y are strongly correlated, though it is unlikely that one would notice the weaker correlation between the parameters w and y , since the values of the parameter w span a much smaller range than do the values of the parameter x . Finally, the parameters w and x also should appear to be uncorrelated, since we stated above that they are physically unrelated. From this information, one can construct the following prior:

$$p(w, x, y|I) = G(w, 0, 0.1)G(x, 0, 1)G(y, x, 0.1), \quad (21)$$

where the last two factors describe the distribution of the data in the x - y plane. Although this prior does not reduce the volume of the solution space as significantly as the above prior does, it

certainly reduces it more than would the prior that one would construct if no correlations were noticed,

$$p(w, x, y|I) = G(w, 0, 0.1)G(x, 0, 1)G(y, 0, 1.005), \quad (22)$$

and it certainly reduces the volume of the solution space significantly more than would the prior one would construct if the prior information were altogether ignored, i.e., if a flat prior were adopted (§2.1.2):

$$p(w, x, y|I) = F(w, w_l, w_u)F(x, x_l, x_u)F(y, y_l, y_u). \quad (23)$$

Here, $w_l < w < w_u$, $x_l < x < x_u$, and $y_l < y < y_u$ define the ranges over which the values of these parameters are considered to be physically plausible.

Example 3. Consider now the related case in which the parameter w either is not or cannot be measured, and in fact, the very relevance of the parameter to the physical process at hand might not even be known. In this case, the prior described by Equation (21) should be replaced by

$$p(w, x, y|I) = F(w, w_l, w_u)G(x, 0, 1)G(y, x, 0.1), \quad (24)$$

if w is one of the model parameters, or by

$$p(x, y|I) = G(x, 0, 1)G(y, x, 0.1), \quad (25)$$

if w is not one of the model parameters.

Example 4. Finally, when constructing priors from data sets, one must be very careful that data selection effects do not bias the priors. For example, suppose that the measured distribution of the parameter values of x merely reflects how the data were sampled, and not how the parameter values of x are intrinsically distributed. In this case, the above prior should be replaced by

$$p(x, y|I) = F(x, x_l, x_u)G(y, x, 0.1). \quad (26)$$

However, in this case, the factor $G(y, x, 0.1)$ is an extrapolation beyond the range of the measured values of the parameter x , and must be treated as such.

When constructing a prior from a multi-dimensional data set in general, we adopt the following procedure: (1) we plot two- and sometimes three-dimensional subsets of the data to facilitate the identification of correlations between parameters; (2) if correlations are found, say between pairs of parameters, we determine the two-dimensional distributions that describe these subsets of the data; we also determine the one-dimensional distributions of the values of all of the parameters; and (3) we use this information to construct a prior for the full parameter space, as in the above examples, while being mindful of data selection effects. How to go about steps (1) and (3) should be clear; how to go about step (2) - the construction of two-dimensional priors, as well as one- and three-dimensional priors - we explain in §2.2.2 and §2.2.3.

2.2.2. Constructing Priors from Two-Dimensional Data Sets

Suppose that two parameters, x and y , are correlated, i.e., that the measured values of these parameters are scattered about a curve, $y = y_c(x; \theta_m)$, where θ_m are M parameters that describe this curve. The scatter of these points about this curve can be both due to measurement errors, in which case the scatter is referred to as *intrinsic* scatter, and due to weaker dependences of either of the parameters x or y on other, yet-unmeasured, and even yet-unknown parameters (e.g., the parameter w in Example 3 of §2.2.1), in which case the scatter is referred to as *extrinsic* scatter. Below, we take all of these scatters to be normally distributed and uncorrelated. Finally, let $g(x, y)\delta(y - y_c)$ be the intrinsic density of points along the curve $y = y_c(x; \theta_m)$, and let $f(x, y)$ be the selection function, i.e., the efficiency at which given values of the parameters x and y are observed. We now construct a prior that describes the correlation between the parameters x and y .

We model the intrinsic density of points in the x' - y' plane by convolving the intrinsic density of points along the curve $y = y_c(x; \theta_m)$, i.e., $g(x, y)\delta(y - y_c)$, with the two-dimensional Gaussian smearing function $G(x', x, \sigma_x)G(y', y, \sigma_y)$, the scale of which is parameterized by 1- σ extrinsic scatters σ_x and σ_y :

$$p_{int}(x', y' | \theta_m, \sigma_x, \sigma_y) = \int_x \int_y g(x, y)\delta(y - y_c)G(x', x, \sigma_x)G(y', y, \sigma_y)dx dy \quad (27)$$

$$= \int_s g(x, y_c)G(x', x, \sigma_x)G(y', y_c, \sigma_y)ds, \quad (28)$$

where $ds = \sqrt{dx^2 + dy_c^2}$ is an element of path length along the length of the curve. The observed density of points in the x' - y' plane is then given by

$$p_{obs}(x', y' | \theta_m, \sigma_x, \sigma_y) = f(x', y')p_{int}(x', y' | \theta_m, \sigma_x, \sigma_y) \quad (29)$$

$$= \int_s f(x', y')g(x, y_c)G(x', x, \sigma_x)G(y', y_c, \sigma_y)ds. \quad (30)$$

The probability distribution of the n th data point, (x_n, y_n) , given 1- σ intrinsic scatters $\sigma_{x,n}$ and $\sigma_{y,n}$, is given by

$$p_n(x', y' | x_n, y_n, \sigma_{x,n}, \sigma_{y,n}) = G_n(x', x_n, \sigma_{x,n})G_n(y', y_n, \sigma_{y,n}). \quad (31)$$

Hence, the joint probability distribution of a given model and the n th data point is given by

$$p_n(x', y' | \theta_m, \sigma_x, \sigma_y, x_n, y_n, \sigma_{x,n}, \sigma_{y,n}) = p_{obs}(x', y' | \theta_m, \sigma_x, \sigma_y)p_n(x', y' | x_n, y_n, \sigma_{x,n}, \sigma_{y,n}) \quad (32)$$

$$= \int_s f(x', y')g(x, y_c)G(x', x, \sigma_x)G(y', y_c, \sigma_y)G_n(x', x_n, \sigma_{x,n})G_n(y', y_n, \sigma_{y,n})ds. \quad (33)$$

The joint probability of a given model, i.e., given values of the parameters θ_m , σ_x , and σ_y , and the n th data point is given by integrating $p_n(x', y' | \theta_m, \sigma_x, \sigma_y, x_n, y_n, \sigma_{x,n}, \sigma_{y,n})$ over x' and y' :

$$p_n(\theta_m, \sigma_x, \sigma_y | x_n, y_n, \sigma_{x,n}, \sigma_{y,n}) =$$

$$\int_{x'} \int_{y'} \int_s f(x', y') g(x, y_c) G(x', x, \sigma_x) G(y', y_c, \sigma_y) G_n(x', x_n, \sigma_{x,n}) G_n(y', y_n, \sigma_{y,n}) dx' dy' ds. \quad (34)$$

Finally, the joint probability of a given model and *all* of the data points is given by taking the product of the N probabilities $p_n(\theta_m, \sigma_x, \sigma_y | x_n, y_n, \sigma_{x,n}, \sigma_{y,n})$:

$$p(\theta_m, \sigma_x, \sigma_y | x_n, y_n, \sigma_{x,n}, \sigma_{y,n}) = \prod_{n=1}^N \int_{x'} \int_{y'} \int_s f(x', y') g(x, y_c) G(x', x, \sigma_x) G(y', y_c, \sigma_y) G_n(x', x_n, \sigma_{x,n}) G_n(y', y_n, \sigma_{y,n}) dx' dy' ds. \quad (35)$$

This is the prior. In this form, it is a function of $M + 2$ parameters: θ_m , σ_x , and σ_y .

If the scale over which the selection function $f(x', y')$ varies from constancy is larger than (1) the scale of the two-dimensional Gaussian $G(x', x, \sigma_x)G(y', y_c, \sigma_y)$, as measured by σ_x and σ_y , and (2) the scale of the two-dimensional Gaussian $G_n(x', x_n, \sigma_{x,n})G_n(y', y_n, \sigma_{y,n})$, as measured by $\sigma_{x,n}$ and $\sigma_{y,n}$, then the first two integrations of Equation (35) can be done analytically:

$$p(\theta_m, \sigma_x, \sigma_y | x_n, y_n, \sigma_{x,n}, \sigma_{y,n}) \approx \prod_{n=1}^N f_n(x_n, y_n) \int_{x'} \int_{y'} \int_s g(x, y_c) G(x', x, \sigma_x) G(y', y_c, \sigma_y) G_n(x', x_n, \sigma_{x,n}) G_n(y', y_n, \sigma_{y,n}) dx' dy' ds = \quad (36)$$

$$\prod_{n=1}^N f(x_n, y_n) \int_s g(x, y_c) G_n(x, x_n, \sqrt{\sigma_x^2 + \sigma_{x,n}^2}) G_n(y, y_n, \sqrt{\sigma_y^2 + \sigma_{y,n}^2}) ds. \quad (37)$$

The final integration, however, is non-trivial. It consists of a path integration through the product of two distributions: $g(x, y)\delta(y - y_c)$, the intrinsic density of points along the curve $y = y(x; \theta_m)$, and the two-dimensional Gaussian $G_n(x, x_n, \sqrt{\sigma_x^2 + \sigma_{x,n}^2}) G_n(y, y_n, \sqrt{\sigma_y^2 + \sigma_{y,n}^2})$. However, if the scale of this two-dimensional Gaussian, as measured by $\sqrt{\sigma_x^2 + \sigma_{x,n}^2}$ and $\sqrt{\sigma_y^2 + \sigma_{y,n}^2}$, is smaller than (1) the scale over which $y_c(x; \theta_m)$ varies from linearity, and (2) the scale over which $g(x, y_c)$ varies from constancy, this integration can be done with relative ease, as we now show.

Let $(x_{t,n}, y_{t,n})$ be the point on the curve $y = y_c(x; \theta_m)$ for which the value of the two-dimensional Gaussian, $G_n(x, x_n, \sqrt{\sigma_x^2 + \sigma_{x,n}^2}) G_n(y, y_n, \sqrt{\sigma_y^2 + \sigma_{y,n}^2})$, is maximum. At this point, the curve $y = y_c(x; \theta_m)$ will be tangent to an iso-contour of the two-dimensional Gaussian, i.e., the ellipse given by

$$\frac{(x - x_n)^2}{\sigma_x^2 + \sigma_{x,n}^2} + \frac{(y - y_n)^2}{\sigma_y^2 + \sigma_{y,n}^2} = \frac{(x_{t,n} - x_n)^2}{\sigma_x^2 + \sigma_{x,n}^2} + \frac{(y_{t,n} - y_n)^2}{\sigma_y^2 + \sigma_{y,n}^2}. \quad (38)$$

By repeatedly setting the slope of this tangential ellipse equal to the slope of the curve, the tangent point, $(x_{t,n}, y_{t,n})$, can be found iteratively; if $y_c(x; \theta_m)$ is indeed slowly varying, only a few iterations are required. Now, making use of the first assumption - that $y_c(x; \theta_m)$ does not vary significantly from linearity over the scale of the two-dimensional Gaussian - one can replace $y_c(x; \theta_m)$ in Equation (37) with the following approximation:

$$y_c(x; \theta_m) \approx y_{t,n} + s_{t,n}(x - x_{t,n}), \quad (39)$$

where

$$s_{t,n} = \left[\frac{\partial y_c(x; \theta_m)}{\partial x} \right]_{x=x_{t,n}} \quad (40)$$

is the slope of $y_c(x; \theta_m)$ (or that of the tangential ellipse) at the tangent point $(x_{t,n}, y_{t,n})$. Finally, by making use of the second assumption - that $g(x, y_c)$ does not vary significantly from constancy over the scale of the two-dimensional Gaussian - one can complete the integration of Equation (37) analytically:

$$\begin{aligned} p(\theta_m, \sigma_x, \sigma_y | x_n, y_n, \sigma_{x,n}, \sigma_{y,n}) &\approx \\ \prod_{n=1}^N f_n(x_n, y_n) g_n(x_n, y_n) \int_s G_n &\left(x, x_n, \sqrt{\sigma_x^2 + \sigma_{x,n}^2} \right) G_n \left(y_c, y_n, \sqrt{\sigma_y^2 + \sigma_{y,n}^2} \right) ds \approx \quad (41) \\ \prod_{n=1}^N f_n(x_n, y_n) g_n(x_n, y_n) \sqrt{1 + s_{t,n}^2} G_n &\left[y_n, y_{t,n} + s_{t,n}(x_n - x_{t,n}), \sqrt{\sigma_y^2 + \sigma_{y,n}^2 + s_{t,n}^2(\sigma_x^2 + \sigma_{x,n}^2)} \right]. \quad (42) \end{aligned}$$

Normalization of the prior removes the need to determine the value of the constant $\prod_{n=1}^N f_n(x_n, y_n) g_n(x_n, y_n)$; hence,

$$\begin{aligned} p(\theta_m, \sigma_x, \sigma_y | x_n, y_n, \sigma_{x,n}, \sigma_{y,n}) &\approx \\ \prod_{n=1}^N \sqrt{1 + s_{t,n}^2} G_n &\left[y_n, y_{t,n} + s_{t,n}(x_n - x_{t,n}), \sqrt{\sigma_y^2 + \sigma_{y,n}^2 + s_{t,n}^2(\sigma_x^2 + \sigma_{x,n}^2)} \right]. \quad (43) \end{aligned}$$

2.2.3. Constructing Practical Priors from Two-Dimensional Data Sets and its Generalization

From the point of view of practicality, Equation (43) has a number of drawbacks. First of all, by formulating the prior in this way, we have replaced the two parameters x and y with $M + 2$, intermediate parameters: θ_m , σ_x , and σ_y . Secondly, potential users of this prior must have access to the $4N$ pieces of prior information, x_n , y_n , $\sigma_{x,n}$, and $\sigma_{y,n}$, where N can be a very large number, that are required for its computation. Finally, the computation of this prior, although completely feasible, is non-trivial: the iterative procedure of finding the tangent point (§2.2.2) must be performed N times at every grid point in the $(M + 2)$ -dimensional space that the prior spans.

These problems can be overcome by instead taking Equation (43) to be a likelihood function, and by then applying the statistical methodology of §2.1.5 to constrain the values of the intermediate parameters θ_m , σ_x , and σ_y , i.e., to reduce the $4N$ pieces of prior information to what we show below to be $2M + 2$ representative values, where M is typically a few. Given these fitted values, it is a simple matter to construct an approximation to Equation (43) (1) that is solely a function of the parameters x and y , (2) that requires only these $2M + 2$ values as prior information, and (3) that is computationally non-taxing. We do this now; we then generalize these results to other dimensions.

Let $\hat{\theta}_m$, $\hat{\sigma}_x$, and $\hat{\sigma}_y$ be the best-fit values of θ_m , σ_x , and σ_y , and let $\hat{\sigma}_{\theta_m}$ be the fitted, 1- σ uncertainties in the values of $\hat{\theta}_m$. If one takes these fitted values to be normally distributed and uncorrelated, Equation (43) may then be approximated by

$$p(x, y | \hat{\theta}_m, \hat{\sigma}_{\theta_m}, \hat{\sigma}_x, \hat{\sigma}_y) \approx G[y, y_c(x; \hat{\theta}_m), \sigma_y(x; \hat{\theta}_m, \hat{\sigma}_{\theta_m}, \hat{\sigma}_x, \hat{\sigma}_y)], \quad (44)$$

where

$$\sigma_y(x; \hat{\theta}_m, \hat{\sigma}_{\theta_m}, \hat{\sigma}_x, \hat{\sigma}_y) = \left\{ \sum_{m=1}^M \left[\sigma_{\theta_m} \frac{\partial y_c(x; \theta_m)}{\partial \theta_m} \right]_{\theta_m=\hat{\theta}_m}^2 + \left[\sigma_x \frac{\partial y_c(x; \theta_m)}{\partial x} \right]_{\theta_m=\hat{\theta}_m}^2 + \sigma_y^2 \right\}^{1/2}. \quad (45)$$

Here, $\sigma_y(x; \hat{\theta}_m, \hat{\sigma}_{\theta_m}, \hat{\sigma}_x, \hat{\sigma}_y)$ is the quadratic sum of the uncertainty in the curve $y = y_c(x; \hat{\theta}_m)$ due to the uncertainties $\hat{\sigma}_{\theta_m}$ in the best-fit values $\hat{\theta}_m$, the uncertainty in the curve $y = y_c(x; \hat{\theta}_m)$ due to the extrinsic scatter $\hat{\sigma}_x$ in the x dimension, and the uncertainty in the curve $y = y_c(x; \hat{\theta}_m)$ due to the extrinsic scatter $\hat{\sigma}_y$ in the y dimension. Consequently, Equation (44) (1) is indeed solely a function of the parameters x and y , (2) requires only $2M + 2$ pieces of prior information, $\hat{\theta}_m$, $\hat{\sigma}_{\theta_m}$, $\hat{\sigma}_x$, and $\hat{\sigma}_y$, and (3) is easily computed.

Equation (44) can be improved upon if the selection function, $f(x, y)$, is well understood. In this case, the intrinsic density of points along the curve $y = y_c(x; \theta_m)$, i.e., $g(x, y_c)$, can be recovered from the observed density of points along the curve $y = y_c(x; \theta_m)$, i.e., $f(x, y_c)g(x, y_c)$, in which case, Equation (44) can be replaced with

$$p(x, y | \hat{\theta}_m, \hat{\sigma}_{\theta_m}, \hat{\sigma}_x, \hat{\sigma}_y) \approx g[x, y_c(x; \hat{\theta}_m)]G[y, y_c(x; \hat{\theta}_m), \sigma_y(x; \hat{\theta}_m, \hat{\sigma}_{\theta_m}, \hat{\sigma}_x, \hat{\sigma}_y)]. \quad (46)$$

However, selection functions often are not well understood, as is the case with the data sets that we present in §4 and §5; consequently, we do not develop this case further in this paper.

One-dimensional priors are trivially derived by setting $s_{t,n} = 0$ in Equation (43). In this case, Equation (44) reduces to:

$$p(y | \hat{y}, \hat{\sigma}_y) = G(y, \hat{y}, \hat{\sigma}_y). \quad (47)$$

Furthermore, it is not difficult to generalize Equations (43) and (44) to more than two dimensions. Let $y = y_c(x_l | \theta_m)$, where $1 \leq l \leq L$. In this case, one can show that Equation (43) generalizes to

$$p(\theta_m, \sigma_{x_l}, \sigma_y | x_{l,n}, y_n, \sigma_{x_{l,n}}, \sigma_{y,n}) \approx \prod_{n=1}^N \sqrt{1 + \sum_{l=1}^L s_{l,t,n}^2} G_n \left[y_n, y_{t,n} + \sum_{l=1}^L s_{l,t,n} (x_{l,n} - x_{l,t,n}), \sqrt{\sigma_y^2 + \sigma_{y,n}^2 + \sum_{l=1}^L s_{l,t,n}^2 (\sigma_{x_l}^2 + \sigma_{x_{l,n}}^2)} \right], \quad (48)$$

where

$$s_{l,t,n} = \left[\frac{\partial y_c(x_l; \theta_m)}{\partial x_l} \right]_{x_l=x_{l,t,n}}, \quad (49)$$

and Equation (44) generalizes to

$$p(x_l, y | \hat{\theta}_m, \hat{\sigma}_{x_l}, \hat{\sigma}_y) \approx G[y, y_c(x_l; \hat{\theta}_m), \sigma_y(x_l; \hat{\theta}_m, \hat{\sigma}_{\theta_m}, \hat{\sigma}_{x_l}, \hat{\sigma}_y)], \quad (50)$$

where

$$\sigma_y(x_l; \hat{\theta}_m, \hat{\sigma}_{\theta_m}, \hat{\sigma}_{x_l}, \hat{\sigma}_y) = \left\{ \sum_{m=1}^M \left[\sigma_{\theta_m} \frac{\partial y_c(x_l; \theta_m)}{\partial \theta_m} \right]_{\theta_m=\hat{\theta}_m}^2 + \sum_{l=1}^L \left[\sigma_{x_l} \frac{\partial y_c(x_l; \theta_m)}{\partial x_l} \right]_{\theta_m=\hat{\theta}_m}^2 + \sigma_y^2 \right\}^{1/2}. \quad (51)$$

3. The Dust Extinction Curve Model

We now present an eight-parameter model that describes the effects of extinction by dust along lines of sight through our galaxy, and by redshifting this model, along lines of sight through burst host galaxies (and along lines of sight through the host galaxies of all extragalactic point sources for that matter). This model is a combination of the two-parameter, IR and optical extinction curve model of Cardelli, Clayton, & Mathis (1989), and the eight-parameter, UV extinction curve model of Fitzpatrick & Massa (1988). We present the IR and optical extinction curve model in §3.1; we present the UV extinction curve model in §3.2. In §3.3, we modify these models to include the effect at far-UV (FUV) wavelengths of absorption by H I in galaxies.

3.1. $\lambda > 3000 \text{ \AA}$

Using UBVRJHKL photometry of 29 reddened Milky Way OB stars (Clayton & Mathis 1988; Clayton & Cardelli 1988), and UV extinction curves that had been fitted to International Ultraviolet Explorer (IUE) spectra of 45 Milky Way OB stars (Fitzpatrick & Massa 1988; see §3.2), Cardelli, Clayton, & Mathis (1988, 1989) constructed an empirical, two-parameter, IR through FUV extinction curve model. The two parameters are A_V and R_V . The former parameter normalizes the extinction curve at the V band; the latter parameter, defined by

$$R_V = \frac{A_V}{E(B-V)} \quad (52)$$

$$= \frac{1}{\frac{A_B}{A_V} - 1}, \quad (53)$$

is a measure of the amount of extinction at the B band relative to that at the V band. The standard diffuse interstellar medium (ISM) value of R_V is 3.1; however, the value of R_V is known to vary with the type of interstellar environment. For example, $R_V \sim 4 - 5$ is typical of dense clouds.

The Cardelli, Clayton, & Mathis (1989) extinction curve is given by:

$$\frac{A_\lambda}{A_V} = a(x) + \frac{b(x)}{R_V}, \quad (54)$$

where $x = (\lambda/1 \mu\text{m})^{-1}$, and $a(x)$ and $b(x)$ are empirical expressions given by

$$a(x) = \begin{cases} 0.574x^{1.61} & (0.3 < x < 1.1) \\ 1 + 0.17699y - 0.50447y^2 - 0.02427y^3 + 0.72085y^4 \\ + 0.01979y^5 - 0.77530y^6 + 0.32999y^7 & (1.1 < x < 3.3) \end{cases} \quad (55)$$

and

$$b(x) = \begin{cases} -0.527x^{1.61} & (0.3 < x < 1.1) \\ 1.41338y + 2.28305y^2 + 1.07233y^3 - 5.38434y^4 \\ - 0.62251y^5 + 5.30260y^6 - 2.09002y^7 & (1.1 < x < 3.3) \end{cases}, \quad (56)$$

where $y = x - 1.82$. Cardelli, Clayton, and Mathis (1989) also determined expressions for $a(x)$ and $b(x)$ in the wavelength range $3.3 < x < 10$ ($1000 \text{ \AA} < \lambda < 3000 \text{ \AA}$); however, the Fitzpatrick & Massa (1988) parameterization of the extinction curve, on which this portion of the Cardelli, Clayton, & Mathis (1989) parameterization of the extinction curve is largely based, is a more general description of the extinction curve in the UV. Consequently, we instead adopt the more general extinction curve model of Fitzpatrick & Massa (1988) at these UV wavelengths (see §3.2).

The extinction curve at wavelengths $\lambda \gtrsim 6000 \text{ \AA}$ is generally attributed to absorption and scattering by classical Van de Hulst grains (Van de Hulst 1957). These are relatively large grains, with sizes of $1000 - 2000 \text{ \AA}$. They are thought to be fluffy, non-spherical composites containing carbon, silicates, oxides, and vacuum (Mathis 1996, 1998; Dwek 1998). Classical grain extinction saturates at a wavelength of $\lambda \sim 3000 \text{ \AA}$.

3.2. $1000 \text{ \AA} < \lambda < 3000 \text{ \AA}$

In a series of four papers, Massa & Fitzpatrick (1986) and Fitzpatrick & Massa (1986, 1988, 1990) measured extinction curves for two samples of reddened Milky Way OB stars from IUE spectra. Their cluster sample consists of 35 stars from five clusters; since these stars were drawn from similar interstellar environments, their extinction curves are relatively similar. Their program sample consists of 45 stars from a wide variety of interstellar environments; consequently, the extinction curves of this sample are more varied. Fitzpatrick & Massa (1988, 1990) found that all 80 extinction curves are well fitted by the following three-component function:

$$\frac{E(\lambda - V)}{E(B - V)} = c_1 + c_2x + c_3D(x; \gamma, x_0) + c_4F(x), \quad (57)$$

where

$$D(x; \gamma, x_0) = \frac{x^2}{(x^2 - x_0^2)^2 + x^2\gamma^2} \quad (58)$$

and

$$F(x) = \begin{cases} 0.5392(x - 5.9)^2 + 0.05644(x - 5.9)^3 & (x > 5.9) \\ 0 & (x < 5.9) \end{cases} . \quad (59)$$

The first component, $c_1 + c_2x$, is linear and spans the wavelength range of the data: $1000 \text{ \AA} < \lambda < 3000 \text{ \AA}$. The second component, $D(x; \gamma, x_0)$, is a functional form called the Drude profile; however, in this context, it is often called the 2175 \AA bump, or the UV bump. The third component, $F(x)$, is an empirical expression called the FUV curvature component, or the FUV non-linear component. We depict all three of these components in Figure 1.

Although the Fitzpatrick & Massa (1988) parameterization of the extinction curve is first and foremost an empirically-driven fitting function, it is not devoid of physical significance. For example, the Drude profile is the functional form of the absorption cross section of a forced-damped harmonic oscillator; it reduces to a Lorentzian near resonance (Jackson 1962). Fitzpatrick & Massa (1986) found that the Drude profile better fits the data than does a pure Lorentzian; Lorentzian profiles had been used previously (Savage 1975; Seaton 1979). The Drude profile is a function of x_0 , the bump’s center, and γ , the bump’s width.

The linear component of the extinction curve is generally attributed to a distribution of grain sizes; the larger grains, with sizes perhaps as large as the classical grains, are responsible for extinction in the near-UV, and the smaller grains, with sizes perhaps as small as 100 \AA or less, are responsible for extinction in the FUV. These grains have been interpreted either as the tail end of the classical grain population (e.g., Mathis, Rumpl, & Nordsieck 1977), or as a separate population altogether (e.g., Hong & Greenberg 1980). The parameters c_1 and c_2 are correlated (see Figure 2, §4.2); however, this correlation is merely an artifact of the fitting procedure by which the values of these parameters are determined (Carnochan 1986, see §4.2).

The values of these parameters are known to vary with the type of interstellar environment. For example, in the diffuse ISM, the values of c_2 are in the range $0.6 - 1$, while in dense clouds, the values of c_2 extend to lower values: $0 - 1$ (e.g., Fitzpatrick & Massa 1988). This difference is generally attributed to the accretion of small grains onto larger grains, or to the coagulation of small grains into larger grains, both of which occur most readily in dense clouds (Scalo 1977; Cardelli, Clayton, & Mathis 1988, 1989; Mathis & Wiffen 1989). In young star-forming regions, like the Orion Nebula, which are also dense clouds, $c_2 \approx 0$ (e.g., Fitzpatrick & Massa 1988). This consistent, low value is generally attributed to stellar radiation forces, or to the evaporation of grains, both of which preferentially remove the smaller grains (McCall 1981; Cardelli & Clayton 1988).

Dense clouds also protect grains from supernovae shocks, which preferentially destroy the larger, classical grains or their mantles, and thus possibly increase the number of grains responsible for the linear component of the extinction curve (Seab & Shull 1983; Jenniskens & Greenberg 1993; Jones, Tielens, & Hollenbach 1996). Since extinction curves are normalized at the V band, the removal of classical grains alone guarantees higher values of c_2 (e.g., Jenniskens & Greenberg

1993). Indeed, in the Large and Small Magellanic Clouds (LMC and SMC), where old star-forming regions, like 30 Doradus (an extreme example), are more common than in the Galaxy, the values of c_2 extend to higher values: 0.6 – 2 for the LMC and the SMC wing, and 2 – 2.5 for the SMC bar (Calzetti, Kinney, & Storchi-Bergmann 1994; Gordon & Clayton 1998; Misselt, Clayton, & Gordon 1999). In starburst galaxies, the values of c_2 are similarly high (Gordon, Calzetti, & Witt 1997).

There is less consensus about the type of grain that is responsible for the UV bump; however, the fact that for fixed values of the IR and optical extinction curve parameter R_V , and of the linear component parameters c_1 and c_2 , the strength of the UV bump can vary considerably, strongly suggests that the classical and linear component grains are not responsible for the UV bump (e.g., Greenberg & Chlewicki 1983). The UV bump is sometimes attributed to small graphitic grains, having diameters of ~ 200 Å or less (e.g., Hecht 1986). One property of this model is that the bump’s width, γ , can vary by a few tens of percent, while its center, x_0 , can vary by only a few percent; this is what is observed (e.g., Fitzpatrick & Massa 1986). Another property of this model is that c_3 and γ are correlated, which is also observed (see Figure 4, §4.2); however, this correlation appears to change with the type of interstellar environment (see §4.2).

Equations (57) and (58) show that the height, or strength, of the UV bump is proportional to c_3/γ^2 . Dense clouds and the diffuse ISM tend to favor strong UV bumps; however, star-forming regions, both young and old, tend to favor weak UV bumps. In fact, in the SMC bar and starburst galaxies, no UV bump is typically observed. Young star-forming regions tend to favor weak UV bumps probably because UV radiation destroys or alters the grains that are responsible for the UV bump (Jenniskens & Greenberg 1993); old star-forming regions tend to favor weak UV bumps probably because UV radiation and/or supernova shocks destroy or alter the grains that are responsible for the UV bump (Gordon, Calzetti, & Witt 1997). These effects can be seen in Figure 5 (see §4.2; see also Clayton, Gordon, & Wolff 2000), where c_3 is an approximate measure of the strength of the UV bump.

Even less is known about the type of grain that is responsible for the FUV non-linear component of the extinction curve. According to the model of Hecht (1986), the small graphitic grains that produce the UV bump should have a second plasmon resonance, resulting in a second and similar bump centered at a wavelength of $\lambda \sim 700 – 800$ Å. Indeed, the shape of the FUV non-linear component resembles the red wing of a Drude profile (Fitzpatrick & Massa 1988). Furthermore, this model suggests that the strengths of these two bumps might be correlated (e.g., Fitzpatrick & Massa 1988); however, hydrogenation of these grains should largely decouple these resonances (e.g., Hecht 1986). Fitzpatrick & Massa (1988) and Jenniskens & Greenberg (1993) have shown that c_3 and γ are both weakly correlated with c_4 ; however, inclusion of the LMC and SMC lines of sight suggests that these correlations also depend on the type of interstellar environment (see Figure 6, §4.2). As in the case of the UV bump parameters, c_4 does not correlate with R_V , c_1 , or c_2 (Jenniskens & Greenberg 1993).

Like the IR and optical extinction curve model of Cardelli, Clayton, & Mathis (1989; Equation 54), the UV extinction curve model of Fitzpatrick & Massa (1988; Equation 57) can be written as a function of A_λ/A_V , given the following rearrangement of the definition of R_V (Equation 52):

$$\frac{A_\lambda}{A_V} = 1 + \frac{1}{R_V} \frac{E(\lambda - V)}{E(B - V)}. \quad (60)$$

To smoothly link these two models (see also Fitzpatrick 1999), we recommend the following weighted average of these models between the V band ($\lambda = 5500$ Å) and $\lambda = 3000$ Å:

$$A_\lambda = \begin{cases} A_{\lambda,CCM} & (x < 1.82) \\ A_{\lambda,CCM} + \frac{x-1.82}{1.48} (A_{\lambda,FM} - A_{\lambda,CCM}) & (1.82 < x < 3.3) \\ A_{\lambda,FM} & (x > 3.3) \end{cases}. \quad (61)$$

To summarize, to the limit of current observations, the IR through FUV extinction curve appears to be most generally modeled by eight parameters: A_V , R_V , c_1 , c_2 , c_3/γ^2 , c_4 , γ , and x_0 ; the UV bump is more naturally parameterized by c_3/γ^2 (bump height) and γ (bump width) than by c_3 and γ , since the former pair is orthogonal (Jenniskens & Greenberg 1993). In §3.3, we modify Equation (61) to include the effect at FUV wavelengths of absorption by H I in galaxies; this does not change the number of parameters. In §4, we show that the volume of the solution space of this additional, but necessary, eight-dimensional parameter space can be reduced significantly, *a priori*, with a prior; without such a prior, Equation (61) has very little predictive power.

3.3. $\lambda < 1000$ Å

The column density of H I in a galaxy along a line of sight is given by

$$N_H = E(B - V)\eta \quad (62)$$

$$= 1.5 \times 10^{21} \text{ cm}^{-2} \left(\frac{A_V}{1 \text{ mag}} \right) \left(\frac{R_V}{3.1} \right)^{-1} \left(\frac{\eta}{\eta_{MW}} \right), \quad (63)$$

where η is the gas to dust ratio of the galaxy along the line of sight, and η_{MW} is the standard value of this ratio for the Milky Way. The bound-free photo-absorption cross section of ground state hydrogen as a function of wavelength is given by

$$\alpha_\lambda = \begin{cases} 7.9 \times 10^{-18} \text{ cm}^2 \left(\frac{\lambda}{912 \text{ Å}} \right)^3 & (\lambda < 912 \text{ Å}) \\ 0 \text{ cm}^2 & (\lambda > 912 \text{ Å}) \end{cases}. \quad (64)$$

Total extinction occurs when $\alpha_\lambda N_H \gg 1$, i.e., when

$$A_V \gg 8.2 \times 10^{-5} \left(\frac{R_V}{3.1} \right) \left(\frac{\eta}{\eta_{MW}} \right)^{-1} \left(\frac{\lambda}{912 \text{ Å}} \right)^{-3} \text{ mag} \quad (65)$$

and $\lambda < 912 \text{ \AA}$. Since this condition is always satisfied along lines of sight through galaxies, at least into the soft X rays, we replace Equation (61) with:

$$A_\lambda = \begin{cases} A_{\lambda,CCM} & (x < 1.82) \\ A_{\lambda,CCM} + \frac{x-1.82}{1.48}(A_{\lambda,FM} - A_{\lambda,CCM}) & (1.82 < x < 3.3) \\ A_{\lambda,FM} & (3.3 < x < 10.96) \\ \infty & (x > 10.96) \end{cases} . \quad (66)$$

Consequently, Equation (66) describes how light is extinguished by dust and absorbed by H I along lines of sight through galaxies, in the rest frame, into the soft X rays.

4. The Dust Extinction Curve Prior

Using fitted extinction curves from Milky Way and Magellanic Cloud lines of sight, and the statistical methodology that we presented in §2, we now construct a prior that weights the eight-dimensional parameter space of the extinction curve model that we presented in §3 such that the volume of the solution space is reduced significantly, *a priori*. We describe the data set in §4.1. We model correlations between extinction curve parameters, and construct the prior, in §4.2.

4.1. The Data Set

From the literature, we have collected the results of fits to 166 extinction curves: we know the values of the UV extinction curve parameters $c_1, c_2, c_3, c_4, \gamma$, and x_0 for all of these lines of sight from fits to IUE spectra; we know the values of the IR and optical extinction curve parameter R_V for 79 of these lines of sight from IR and optical photometry. These lines of sight sample a wide variety of interstellar environments in the Milky Way, the LMC, and the SMC. We describe the breakdown of the data set in detail below; we summarize this information in Table 1.

Ideally, we would fit the models of correlations between extinction curve parameters that we present in §4.2 directly to the IUE spectra and IR and optical photometry, instead of to the fitted values of the extinction curve parameters, which represent a compression of the information contained in the actual data. However, to do so would not be practicable. Consequently, we instead adopt the best-fit values of the extinction curve parameters, $c_1, c_2, c_3, c_4, \gamma, x_0$, and R_V , and the fitted uncertainties in these parameters, when available, as the data set, at the expense of a minor loss of information.

We have drawn the results of fits to Galactic extinction curves from two sources: the cluster and program samples of Fitzpatrick & Massa (1990) and the sample of Jenniskens & Greenberg (1993). The FM cluster sample consists of 35 fitted extinction curves, the FM program sample consists of 45 fitted extinction curves, and the JG sample consists of 115 fitted extinction curves. For information about how these samples were selected, and about how the selected, IUE spectra

were fitted, we refer the reader to these papers. There is some overlap between these samples: 3 of the FM cluster sample extinction curves and 24 of the FM program sample extinction curves are also in the the JG sample. This lowers the number of Galactic extinction curves in our sample from 195 to 168. Of these extinction curves, Jenniskens & Greenberg (1993) deemed 25 to be of low quality (see Jenniskens & Greenberg 1993 for details). This lowers the number of Galactic extinction curves in our sample to 143.

Of the 39 FM program sample lines of sight with high quality extinction curves, Cardelli, Clayton, & Mathis (1989) found values of R_V for 25 of these lines of sight from BVRIJHKL photometry. Of the 90 JG sample lines of sight with high quality extinction curves, Aiello et al. (1988) found values of R_V for 49 of these lines of sight from BVK photometry. Eight of these lines of sight are in common. This lowers the number of Galactic values of R_V from 74 to 66.

From the fitted parameter values of the 21 high quality extinction curves that the FM and JG samples have in common, Jenniskens & Greenberg (1993) measured systematic and random errors between the two group's fitted values for each extinction curve parameter; we list these errors in Table 2. Furthermore, these systematic and random errors are comparable in size. In the interest of creating a uniform data set, primarily to facilitate identification and modeling of the correlations between these parameters, we have shifted each group's fitted parameter values by one half of the systematic difference between the two group's results; this brings both group's results into general agreement. We re-inject these systematic errors into the analysis in §4.2.

Secondly, unlike the fitted parameter values of the LMC and SMC extinction curves, which we introduce below, uncertainties were not determined for each, or any, of the fitted parameter values of the Galactic extinction curves. Consequently, we adopt the above measured random errors as indicative of the uncertainties in the fitted parameter values of each of the Galactic extinction curves in our sample. Technically, since both groups fitted to the same IUE spectra, these random errors are lower limits. However, Massa & Fitzpatrick (1986) measured nearly identical upper limits from variations in the fitted parameter values of extinction curves measured along different lines of sight in the same OB associations; we list these errors in Table 2 also. We adopt the lower limits because this forces us to conservatively overestimate the extrinsic scatters in the fits of §4.2.

To our Galactic sample, we have added the results of fits to 19 extinction curves, and 10 corresponding values of R_V , from the LMC (Misselt, Clayton & Gordon 1999), and the results of fits to 4 extinction curves, and 3 corresponding values of R_V , from the SMC (Gordon & Clayton 1998). This raises the number of extinction curves in our sample to 166, and the number of corresponding values of R_V to 79. Uncertainties have been determined for each of the fitted parameter values of the LMC and SMC extinction curves.

4.2. Correlations between Dust Extinction Curve Parameters

We now model known correlations between the pairs of extinction curve parameters c_1 and c_2 , and R_V and c_2 . We also present possible correlations between the triplets of extinction curve parameters c_3 , γ , and c_2 ; c_4 , c_3 , and c_2 ; and c_4 , γ , and c_2 ; however, we consider these three-parameter correlations to be too speculative to incorporate into our extinction curve prior. We also constrain the values of the extinction curve parameters γ and x_0 , which do not vary significantly across all 166 of the lines of sight in our data set (§4.1). Finally, we use this information to construct the extinction curve prior.

We begin with a discussion of the extinction curve parameter c_2 , upon which all of the above correlations depend. In §3.2, we pointed out that different values of c_2 are measured from different interstellar environments: low values of c_2 are measured from young star-forming regions, low to moderate values of c_2 are measured from dense clouds, moderate values of c_2 are measured from the diffuse ISM, and moderate to high values of c_2 are measured from old star-forming regions. This is not to say that c_2 is a good measure of an interstellar environment’s type: e.g., 30 Doradus is roughly ten times as active of a star-forming region as any region in the SMC (Caplan et al. 1996), yet significantly higher values of c_2 are measured from the SMC bar than from 30 Doradus; this is probably due to the SMC having lower density clouds, which are less able to protect the classical grains from UV radiation and supernovae shocks, than does the LMC (Misselt, Clayton, & Gordon 1999). However, c_2 might be a reasonable, approximate measure of the net ability of an interstellar environment to affect extinguishing grains. Hence, the above correlations might be viewed as how the values of other extinction curve parameters, or the correlations between other extinction curve parameters, vary as a function of a single-parameter measure of net environmental conditions.

To apply the statistical methodology that we presented in §2.2, (1) the models that we adopt to describe the above correlations must be slowly varying, i.e., the curve $y = y_c(x; \theta_m)$ from §2.2.2 and §2.2.3 must be varying from linearity only on scales that are larger than the scales given by the scatter of the data that we presented in §4.1 about this curve; and (2) the density of these data along this curve also must be slowly varying; i.e., the intrinsic density along this curve, $g(x, y_c)$, and the selection function, $f(x, y)$, must be varying from constancy only on scales that are larger than the scales given by this scatter of the data (§2.2.2). As we adopt only constant, linear, and slowly-varying quadratic models below, the first condition is met. As for the second condition, the density of the data varies most obviously with the value of c_2 . This is probably due to the selection function; e.g., diffuse ISM lines of sight, and consequently, values of $c_2 \sim 0.8$, have been selected more often than lines of sight through any other type of interstellar environment, or value of c_2 . These density variations, however, also occur on scales that are larger than the scales given by the scatter of the data; consequently, the second condition also appears to be met. Hence, we appear to be within the realm of the formalism that we presented in §2.2, with but one caveat. The intrinsic scatters of some of the extinction parameters, namely c_1 and c_2 , are probably somewhat correlated (Fitzpatrick & Massa 1988). This causes us to somewhat underestimate the

extrinsic scatters of these correlations below, but not significantly.

We begin with the two-parameter correlations: c_1 and c_2 (Figure 2), and R_V and c_2 (Figure 3). In both cases, the parameters are well correlated; however, both of these correlations are more mathematical than physical in nature. In the case of the former correlation, the linear component of Equation (57) is observed to pivot about a point at a wavelength of $\lambda \approx 3000$ Å as the slope, c_2 , of this component changes from one line of sight to another. If c_1 were measured at this wavelength, instead of at $\lambda = \infty$, this correlation would disappear; consequently, this correlation is merely an artifact of the fitting procedure by which the values of these parameters were determined (Carnochan 1986), and not due to any intrinsic physical property. However, the small size of the extrinsic scatter that we measure below for this correlation testifies to the constancy of the extinction curve at this pivot point. This is a physical property, since the wavelength of this pivot point differs from the V-band wavelength, $\lambda \approx 5500$ Å, at which the extinction curve is normalized.

To the degree that the IR and optical extinction curve is really a one-parameter function of R_V , and to the degree that the linear component of the UV extinction curve is really a one-parameter function of c_2 (since c_1 and c_2 are strongly correlated), R_V and c_2 must be correlated if the extinction curve is to be continuous and differentiable between optical and UV wavelengths; consequently, this relation is also mathematical in nature. However, physical information can be gleamed from the value of R_V , which by Equation (53) is a measure of the relative numbers and/or absorptivities of grains extinguishing in the B band to grains extinguishing in the V band. How this value changes as the value of c_2 is changed provides physical information, perhaps as a function of environmental conditions, as we have discussed above.

We now model these two correlations, and construct the prior, as described in §2.2.2 and §2.2.3. We do not include the Orion Nebula lines of sight in either of these fits, because nebular background contamination artificially lowers the measured values of c_1 along these lines of sight (Panek 1983), and similarly may affect the measured values of c_2 (Fitzpatrick & Massa 1988); this effect has not been corrected for in these data (Fitzpatrick & Massa 1988).

Given how the values of c_1 and c_2 were determined, we model the first of these correlations with a function that is linear in c_2 :

$$c_1(c_2) = b + m(c_2 - \bar{c}_2), \quad (67)$$

where \bar{c}_2 is the sample's median value of c_2 . The $1-\sigma$ uncertainty in c_1 as a function of c_2 is approximately given by

$$\sigma_{c_1}(c_2) = \left[\left(\sigma_b \frac{\partial c_1}{\partial b} \right)^2 + \left(\sigma_m \frac{\partial c_1}{\partial m} \right)^2 + (\sigma_{c_1})^2 + \left(\sigma_{c_2} \frac{\partial c_1}{\partial c_2} \right)^2 \right]^{1/2}, \quad (68)$$

where σ_b and σ_m are the fitted $1-\sigma$ uncertainties in the parameters b and m , and σ_{c_1} and σ_{c_2} are the fitted $1-\sigma$ extrinsic scatters in the c_1 and c_2 dimensions (§2.2.3). Assuming a flat prior, we find:

$\bar{c}_2 = 0.711$, $b = -0.064$, $\sigma_b = 0.026$, $m = -3.275$, $\sigma_m = 0.083$, $\sigma_{c_1} = 0.088$, and $\sigma_{c_2} = 0.008$. Using Equation (68) and these fitted values, we plot approximate 1-, 2-, and 3- σ confidence regions in Figure 2. Re-injection of the systematic errors between the FM and JG samples that we removed in §4.1 (Table 2) increases σ_{c_1} to 0.176 and σ_{c_2} to 0.037.

The R_V - c_2 correlation clearly is non-linear; however, it is slowly varying, so we model it with a function that is quadratic in c_2 :

$$R_V(c_2) = b + m(c_2 - \bar{c}_2) + n(c_2 - \bar{c}_2)^2. \quad (69)$$

The 1- σ uncertainty in R_V as a function of c_2 is approximately given by

$$\sigma_{R_V}(c_2) = \left[\left(\sigma_b \frac{\partial R_V}{\partial b} \right)^2 + \left(\sigma_m \frac{\partial R_V}{\partial m} \right)^2 + \left(\sigma_n \frac{\partial R_V}{\partial n} \right)^2 + (\sigma_{R_V})^2 + \left(\sigma_{c_2} \frac{\partial R_V}{\partial c_2} \right)^2 \right]^{1/2}, \quad (70)$$

where σ_n is the fitted 1- σ uncertainty in the parameter n , and σ_{R_V} is the fitted 1- σ extrinsic scatter in the R_V dimension. Assuming a flat prior, we find: $\bar{c}_2 = 0.721$, $b = 3.228$, $\sigma_b = 0.053$, $m = -2.685$, $\sigma_m = 0.159$, $n = 1.806$, $\sigma_n = 0.129$, $\sigma_{R_V} = 0.000$, and $\sigma_{c_2} = 0.142$. Using Equation (70) and these fitted values, we plot approximate 1-, 2-, and 3- σ confidence regions in Figure 3. Re-injection of the systematic errors between the FM and JG samples increases σ_{R_V} to 0.112 and σ_{c_2} to 0.147.

We now consider the three-parameter correlation c_3 , γ , and c_2 (Figure 4). A strong correlation exists between c_3 and γ for Galactic lines of sight ($c_2 \sim 2/3$) (Fitzpatrick & Massa 1988; Jenniskens & Greenberg 1993); however, inclusion of the Orion Nebula-like lines of sight ($c_2 \sim 0$), and the LMC and SMC wing lines of sight ($c_2 \sim 4/3$) ruins this previously-determined correlation; the SMC bar lines of sight ($c_2 \sim 7/3$) are not constraining since γ cannot be well determined when $c_3 \sim 0$. These lines of sight request a shallower relation. Physically, this probably corresponds to the destruction or alteration of the UV bump grains by UV radiation and/or supernovae shocks (§3.2, Figure 5; see also Clayton, Gordon, & Wolff 2000).

Weak correlations exist between c_4 and c_3 , and c_4 and γ for Galactic lines of sight (Fitzpatrick & Massa 1988; Jenniskens & Greenberg 1993); indeed, weak positive correlations can be seen in Figure 6, if only the Galactic lines of sight are considered. However, inclusion of the LMC and SMC lines of sight also ruins these previously-determined correlations. The destruction or alteration of UV bump grains by the environment probably accounts for the shift to lower values of c_3 in the top panel of Figure 6. Hydrogenation might account for the greater scatter in the bottom panel of Figure 6 (§3.2).

In any case, we do not attempt to model and constrain the possible correlations in Figures 4, 5, and 6. First of all, in distant galaxies, these grain species might occur in different relative abundances, perhaps due to different relative metallicities. Secondly, even if this is not the case, if the extinction is due primarily to dust that is local to the burst, the relative abundances of these grain species may be altered by the burst itself, as well as by the afterglow (Lamb & Reichart

2000b). Consequently, no constraint can be placed between the extinction curve parameters c_2 , c_3/γ^2 , and c_4 .

The values of γ and x_0 are approximately constant across all 166 lines of sight. We find their values to be $\gamma = 0.958 \pm 0.088$ and $x_0 = 4.593 \pm 0.020$. Since the width of the UV bump is approximately equal to the widths of the photometric bands ($\Delta\nu/\nu \approx 0.2$), and since the uncertainty in the center of the UV bump is significantly smaller than the widths of the photometric bands ($\Delta\nu/\nu \approx 0.004 \ll 0.2$), when fitting to afterglow photometry, precise values of these parameters cannot be extractable from the data; i.e., the fitted solutions should largely resemble the adopted prior, particularly in the case of the bump center parameter, x_0 .

We now construct from these results an extinction curve prior, in accordance with the examples of §2.2.1. For the extinction curve parameters R_V , c_1 , c_2 , γ , and x_0 , we recommend that the following prior be used:

$$p(R_V, c_1, c_2, \gamma, x_0 | I) = G[R_V, R_V(c_2), 3\sigma_{R_V}(c_2)]G[c_1, c_1(c_2), 3\sigma_{c_1}(c_2)] \\ \times G(\gamma, 0.958, 0.264)G(x_0, 4.593, 0.060). \quad (71)$$

Here, we have conservatively tripled the $1-\sigma$ uncertainties of the component priors, simply because these priors are determined solely from information that is local to our galaxy. For the extinction curve parameters A_V , c_3/γ^2 , and c_4 , we conservatively recommend that a flat prior be used. Altogether, this prior weights the eight-dimensional parameter space of the extinction curve model that we presented in §3 such that the volume of the solution space is reduced significantly, *a priori*.

Finally, we comment on the possibility of an evolving extinction curve. As mentioned above, if an afterglow is extinguished by dust that is local to a burst, energetic photons, both from the burst and from the afterglow, may alter the extinction curve with time (Lamb & Reichart 2000b). However, since all afterglows observed to date have faded more rapidly than $F_\nu \sim t^{-1}$ at optical through X-ray wavelengths, the majority of these energetic photons are probably emitted during the first few seconds or minutes of the afterglow, if not during the burst itself. Hence, any dust destruction or alteration that may occur, should occur on such timescales. By restricting oneself to photometry taken hours or longer after a burst, one should be able to safely ignore the possibility of an evolving extinction curve.

5. The Ly α Forest Flux Deficit Model and Prior

At redshifts of $z \gtrsim 2$, the Ly α forest will absorb light at optical wavelengths, and consequently cannot be ignored (Fruchter 1999a; Lamb & Reichart 2000a). We present a two-parameter model that describes the effects of the Ly α forest on the spectral flux distributions of afterglows (and on the spectral flux distributions of all extragalactic point sources for that matter). Using Ly α forest flux deficit measurements from quasar absorption line systems, we construct a prior that weights this two-dimensional space such that the volume of the solution space is reduced significantly.

In the study of quasar absorption line systems, the quantity called flux deficit, denoted D_A , is defined by

$$D_A = \left\langle 1 - \frac{F_\nu(\text{observed})}{F_\nu(\text{continuum})} \right\rangle, \quad (72)$$

where this quantity is averaged over the wavelength range between the emission lines Ly α and Ly β + O VI that is not affected by emission line wings, and only if the continuum can be reliably extrapolated from the unabsorbed spectrum at longer wavelengths (Oke & Korycansky 1982). Zuo & Phinney (1993), Zuo (1993), and Lu & Zuo (1994) model this quantity by

$$D_A(z) \approx 1 - \exp \left[-a \left(\frac{1+z}{1+\bar{z}} \right)^b \right], \quad (73)$$

where a and b are parameters whose values are determined by fitting to flux deficit measurements, z is the redshift corresponding to the central wavelength of the range over which the quantity D_A is averaged, and \bar{z} is the median value of z for the sample to which one is fitting. The 1- σ uncertainty in D_A as a function of z is approximately given by

$$\sigma_{D_A}(z) = \left[\left(\sigma_a \frac{\partial D_A}{\partial a} \right)^2 + \left(\sigma_b \frac{\partial D_A}{\partial b} \right)^2 + (\sigma_{D_A})^2 + \left(\sigma_z \frac{\partial D_A}{\partial z} \right)^2 \right]^{1/2}, \quad (74)$$

where σ_a and σ_b are the fitted 1- σ uncertainties in the parameters a and b , and σ_{D_A} and σ_z are the fitted 1- σ extrinsic scatters in the D_A and z dimensions (§2.2.3).

Assuming a flat prior, and adopting Sample 4 of Zuo & Lu (1993), which is a combination of Sample 2 of Zuo & Lu (1993) (see Zuo & Lu 1993 for details) and the high redshift ($z \sim 4$) sample of Schneider, Schmidt, & Gunn (1989a,b, 1991), we find: $\bar{z} = 2.994$, $a = 0.306$, $\sigma_a = 0.010$, $b = 4.854$, $\sigma_b = 0.188$, $\sigma_{D_A} = 0.000$, and $\sigma_z = 0.165$. We plot Sample 4 of Zuo and Lu (1993) and, using Equation (74) and these fitted values, approximate 1-, 2-, and 3- σ confidence regions in Figure 7. The extent of the scatter about the best fit in Figure 7 is largely a reflection of the extent of the wavelength range over which these values of D_A were averaged. This wavelength range corresponds to $\Delta\nu/\nu \approx 0.2$, which is typical of the photometric bands. In other words, the scatter in Figure 7, very conveniently, is typical of what one would find if Ly α forest flux deficits were measured from afterglows photometrically. Consequently, the Ly α forest flux deficit prior *for photometric, as opposed to spectroscopic, data* is given by (§2.2.1)

$$p(D_A, z | I) = G[D_A, D_A(z), \sigma_{D_A}(z)]. \quad (75)$$

6. Example Extinguished and Absorbed Spectral Flux Distributions

We now demonstrate the breath of the models of §3 and §5. Using these models, we plot in Figure 8 example spectral flux distributions that have been extinguished by dust in a host galaxy, absorbed by H I in the host galaxy, redshifted, and absorbed by the Ly α forest, for a wide variety

of plausible extinction curves and redshifts. We have adopted an intrinsic spectrum of $F_\nu \propto \nu^{-1}$, and we allow the values of A_V , c_2 , c_3/γ^2 , c_4 , and z to vary over observed/reasonable ranges. The values of R_V , c_1 , γ , x_0 , and D_A , we take from the best fits of §4.2 and §5. Finally, we convolve each extinguished, absorbed, and redshifted spectrum with a logarithmically flat smearing function of width $\Delta\nu = 0.2\nu$, converting each spectrum to a spectral flux distribution; i.e., we model how these spectra would be sampled photometrically, as opposed to spectroscopically (§5). Clearly, a single intrinsic spectrum can manifest itself in a multitude of ways, and exhibit a variety of broad spectral features, including a shoulder in the infrared, the UV bump, the Ly α forest, and the Lyman limit.

7. Conclusions

In this paper, we have presented a very general, Bayesian inference formalism with which afterglow models can be tested, and with which the parameter values of acceptable models can be constrained. Furthermore, we have developed and presented a formalism for the construction of Bayesian prior probability distributions from multi-dimensional data sets, which we have drawn on extensively. We have presented models that describe how extinction by dust, both in host galaxies and in our galaxy, and absorption by the Ly α forest and by H I in host galaxies, change the intrinsic spectra of afterglows. Then, applying the above formalism, we constructed a prior that weights the additional, but necessary, parameter space of these models such that the volume of the solution space is reduced significantly, *a priori*. These models and priors will lead to the more realistic modeling of afterglows, particularly at IR through UV wavelengths, in future papers.

Finally, we emphasize that the phenomena for which we have presented models and priors in this paper – extinction by dust and absorption by the Ly α forest – affect identically the light from all other extragalactic point sources.⁵ Consequently, the work presented in this paper is as applicable to high-redshift Type Ia supernovae and quasars, for example, as it is to the afterglows of bursts. Since the effects of extinction and absorption are most dramatic at UV wavelengths in the source frame, these models and priors will be particularly useful for the modeling of optical

⁵By point source, we mean either that the host galaxy contributes a negligible fraction of the total light within the point spread function of the point source, or that this contribution of the host galaxy to the total light can be measured directly – which can be done in the case of a fading point source after it fades away – and consequently separated from that of the point source. Otherwise, one must model not a single point source in a distribution of dust, but instead a distribution of point sources in a distribution of dust, which is a significantly more challenging endeavor, but certainly not impossible (e.g., Witt, Thronson, & Capuano 1992; Gordon, Calzetti, & Witt 1997). Similarly, light from a point source that is either scattered or absorbed and thermally re-emitted into the line of sight can contribute non-negligibly to, and even dominate the direct light of a fading point source at late times, due to the time delay with which the indirect light is received (e.g., Reichart 2000). Again, one must either use data from early times, when the contribution of the “dust echo” is negligible, or measure the contribution of the dust echo at late times, when the contribution of the fading point source is negligible, and use this information to properly interpret the data at intermediate times, when neither component can be ignored.

photometry of high-redshift point sources.

Support for this work was provided by NASA through the Hubble Fellowship grant #HST-SF-01133.01-A from the Space Telescope Science Institute, which is operated by the Association of Universities for Research in Astronomy, Inc., under NASA contract NAS5-26555. Support for this work was also provided by NASA contracts NASW-4690 and SCSV 464006. I am very grateful to C. Graziani, D. Q. Lamb, and M. C. Miller, in particular for many discussions that we had concerning the Bayesian inference techniques presented in this paper. I am also grateful to S. Burles for discussions that we had concerning the modeling of the Ly α forest flux deficit measurements, and to A. N. Witt for discussions that we had concerning the physical nature of the grain species.

REFERENCES

- Aiello, S., et al. 1988, *A&A*, 73, S195
- Bloom, J. S., et al. 1998, *ApJ*, 508, L21
- Bloom, J. S., et al. 1999a, *ApJ*, 518, L1
- Bloom, J. S., et al. 1999b, *Nature*, 401, 453
- Calzetti, D., Kinney, A. L., & Storchi-Bergmann, T. 1994, *ApJ*, 429, 582
- Caplan, J., et al. 1996, *A&A*, 307, 403
- Cardelli, J. A., & Clayton, G. C. 1988, *AJ*, 95, 516
- Cardelli, J. A., Clayton, G. C., & Mathis, J. S. 1988, *ApJ*, 329, L33
- Cardelli, J. A., Clayton, G. C., & Mathis, J. S. 1989, *ApJ*, 345, 245
- Carnochan, D. J. 1986, *MNRAS*, 219, 903
- Clayton, G. C., & Cardelli, J. A. 1988, *AJ*, 96, 695
- Clayton, G. C., Gordon, K. D., & Wolff, M. J. 2000, *ApJ*, 129, S147
- Clayton, G. C., & Mathis, J. S. 1988, *ApJ*, 327, 911
- Djorgovski, S. G., et al. 1998a, GCN Report 114
- Djorgovski, S. G., et al. 1998b, GCN Report 117
- Djorgovski, S. G., et al. 1998c, GCN Report 189
- Djorgovski, S. G., et al. 1998d, *ApJ*, 508, L17
- Dwek, E. 1998, *ApJ*, 501, 643
- Fitzpatrick, E. L. 1999, *PASP*, 111, 63
- Fitzpatrick, E. L., & Massa, D. 1986, *ApJ*, 307, 286
- Fitzpatrick, E. L., & Massa, D. 1988, *ApJ*, 328, 734
- Fitzpatrick, E. L., & Massa, D. 1990, *ApJ*, 72, S163
- Fruchter, A. S. 1999a, *ApJ*, 512, L1
- Fruchter, A. S. 1999b, private communication
- Fruchter, A. S. 1999c, private communication

- Fruchter, A. S., et al. 1999a, *ApJ*, 516, 683
- Fruchter, A. S., et al. 1999b, *ApJ* (Letters), submitted (astro-ph/9903236)
- Fruchter, A. S., et al. 1999c, *ApJ*, 519, L13
- Gordon, K. D., Calzetti, D., & Witt, A. N. 1997, *ApJ*, 487, 625
- Gordon, K. D., & Clayton, G. C. 1998, *ApJ*, 500, 816
- Greenberg, J. M., & Chlewski, G. 1983, *ApJ*, 272, 563
- Hjorth, J., et al. 1999, GCN Report 403
- Hecht, J. H. 1986, *ApJ*, 305, 817
- Hong, S. S., & Greenberg, J. M. 1980, *A&A*, 88, 194
- Jackson, J. D. 1962, “Classical Dynamics” (New York: Wiley)
- Jenniskens, P., & Greenberg, J. M. 1993, *A&A*, 274, 439
- Jones, A. P., Tielens, G. G. M., & Hollenbach, D. J. 1996, *ApJ*, 469, 740
- Kulkarni, S. R., et al. 1998, *Nature*, 393, 35
- Lamb, D. Q. 1999, *A&A*, 138, S607
- Lamb, D. Q., & Reichart, D. E., 2000a, *ApJ*, 536, 1
- Lamb, D. Q., & Reichart, D. E., 2000b, in prep.
- Loredo, T. J. 1992, in “Statistical Challenges in Modern Astronomy”, eds., E. Feigelson & G. Babu (New York: Springer-Verlag)
- Lu, L., & Zuo, L. 1994, *ApJ*, 426, 502
- Massa, D., & Fitzpatrick, E. L. 1986, *ApJ*, 60, S305
- Mathis, J. S. 1996, *ApJ*, 472, 643
- Mathis, J. S. 1998, *ApJ*, 497, 824
- Mathis, J. S., Rumpl, W., Nordsieck, K. H. 1977, *ApJ*, 217, 425
- Mathis, J. S., & Wiffen, G. 1989, *ApJ*, 341, 808
- McCall, M. L. 1981, *MNRAS*, 194, 485
- Misselt, K. A., Clayton, G. C., & Gordon, K. D. 1999, *ApJ*, 515, 128

- Oke, J. B., & Korycansky, D. G. 1982, *ApJ*, 255, 11
- Panek, R. J. 1983, *ApJ*, 270, 169
- Reichart, D. E. 1997, *ApJ*, 495, L99
- Reichart, D. E. 2000, in prep.
- Sahu, K. C., et al. 1997, *Nature*, 387, 476
- Savage, B. D. 1975, *ApJ*, 199, 92
- Scalo, J. M. 1977, *A&A*, 55, 253
- Seab, C. G., & Shull, J. M. 1983, *ApJ*, 275, 652
- Seaton, M. J. 1979, *MNRAS*, 187, P73
- Schneider, D. P., Schmidt, M., & Gunn, J. E. 1989a, *AJ*, 98, 1507
- Schneider, D. P., Schmidt, M., & Gunn, J. E. 1989b, *AJ*, 98, 1951
- Schneider, D. P., Schmidt, M., & Gunn, J. E. 1991, *AJ*, 102, 837
- Van de Hulst, H. C. 1957, “Scattering by Small Particles” (New York: Wiley)
- Witt, A. N., Thronson, H. A., & Capuano, J. M. 1992, *ApJ*, 393, 611
- Zuo, L., & Lu, L. 1993, *ApJ*, 418, 601
- Zuo, L., & Phinney, E. S. 1993, *ApJ*, 418, 28

Table 1. Breakdown of the Extinction Curve Data Set

Galaxy	Extinction Curve Sample ^a	Number of Extinction Curves	Number of Values of R_V	R_V Reference ^a
MW	FM Cluster	35	0	
	FM Program	45	25	CCM
	JG	115	49	Aea
	Combined ^b	143	66	
LMC	MCG	19	10	MCG
SMC	GC	4	3	GC
Combined	Combined	166	79	

^aFM – Fitzpatrick & Massa 1990; JG – Jenniskens & Greenberg 1993; MCG – Misselt, Clayton, & Gordon 1999; GC – Gordon & Clayton 1998; CCM – Cardelli, Clayton, & Mathis 1989; Aea – Aiello et al. 1988.

^bOverlap between the samples, and low quality data have been removed (see §4.1 for details).

Table 2. Systematic and Random Errors Between the FM and JG Samples

Parameter	Systematic Error ^{a,b}	Random Error Lower Limit ^b	Random Error Upper Limit ^c
c_1	0.304	0.259	
c_2	-0.073	0.050	0.08
c_3	0.316	0.252	0.27
c_4	0.082	0.063	0.08
γ	0.036	0.039	0.04
x_0	-0.013	0.010	0.01
R_V	-0.224	0.205	

^aJG – FM

^bBased on the 20 non-Orion Nebula, high quality extinction curves that the FM and JG samples have in common (see §4.1 for details).

^cBased on variations along different lines of sight in the same OB associations (see §4.1 for details). From Table 2 of Jenniskens & Greenberg 1993.

Fig. 1.— An extinction curve that is typical of the diffuse ISM of our galaxy. The dotted lines mark the three components of the UV extinction curve of Fitzpatrick & Massa (1988) (see §3.2).

Fig. 2.— The correlation between the extinction curve parameters c_1 and c_2 . The dotted lines mark approximate 1-, 2- and 3- σ confidence regions (see §4.2). The filled squares are from the Fitzpatrick & Massa (1988; FM) cluster sample, the filled circles are from the FM program sample, the empty triangles are from the Jenniskens & Greenberg (1993; JG) sample, the empty squares are from both the FM cluster sample and the JG sample, the empty circles are from both the FM program sample and the JG sample, the solid error bars denote the Misselt, Clayton, & Gordon (1999) LMC sample, and the dotted error bars denote the Gordon & Clayton (1998) SMC sample (see §4.1). The error bars of the Galactic points are discussed in §4.1. The encircled points denote lines of sight through the Orion Nebula region.

Fig. 3.— The correlation between the extinction curve parameters R_V and c_2 . The dotted lines mark approximate 1-, 2- and 3- σ confidence regions (see §4.2, Figure 2).

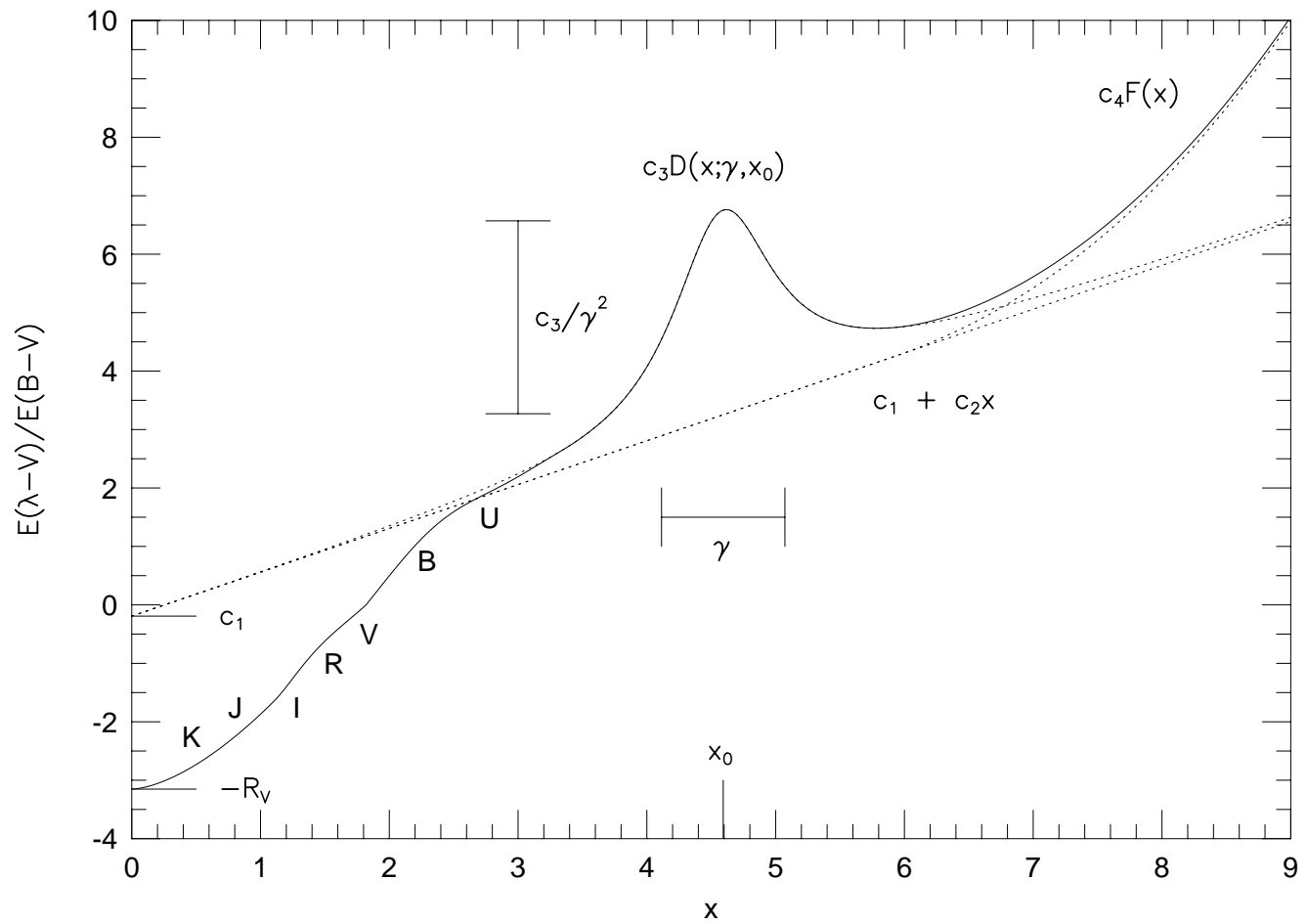
Fig. 4.— The correlation between the extinction curve parameters c_3 and γ as a function of c_2 : the Orion Nebula region lines of sight have $c_2 \sim 0$, the Galactic lines of sight have $c_2 \sim 2/3$, the LMC and SMC wing lines of sight have $c_2 \sim 4/3$, and the SMC bar lines of sight have $c_2 \sim 7/3$ (see §4.2, Figure 2).

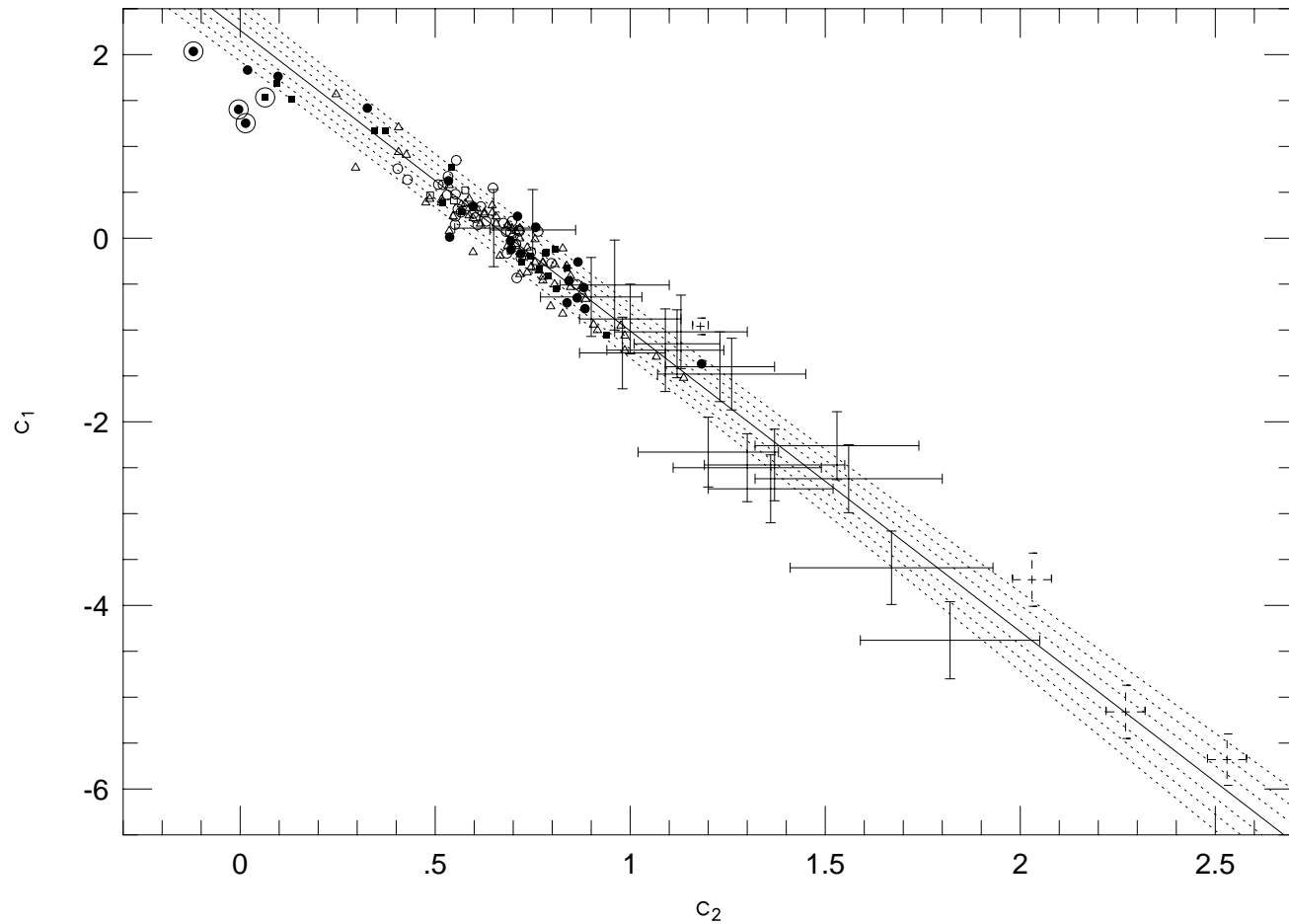
Fig. 5.— How the strength of the UV bump, as measured by c_3 , varies with environmental conditions, as measured by c_2 (see §3.2, §4.2, Figure 2).

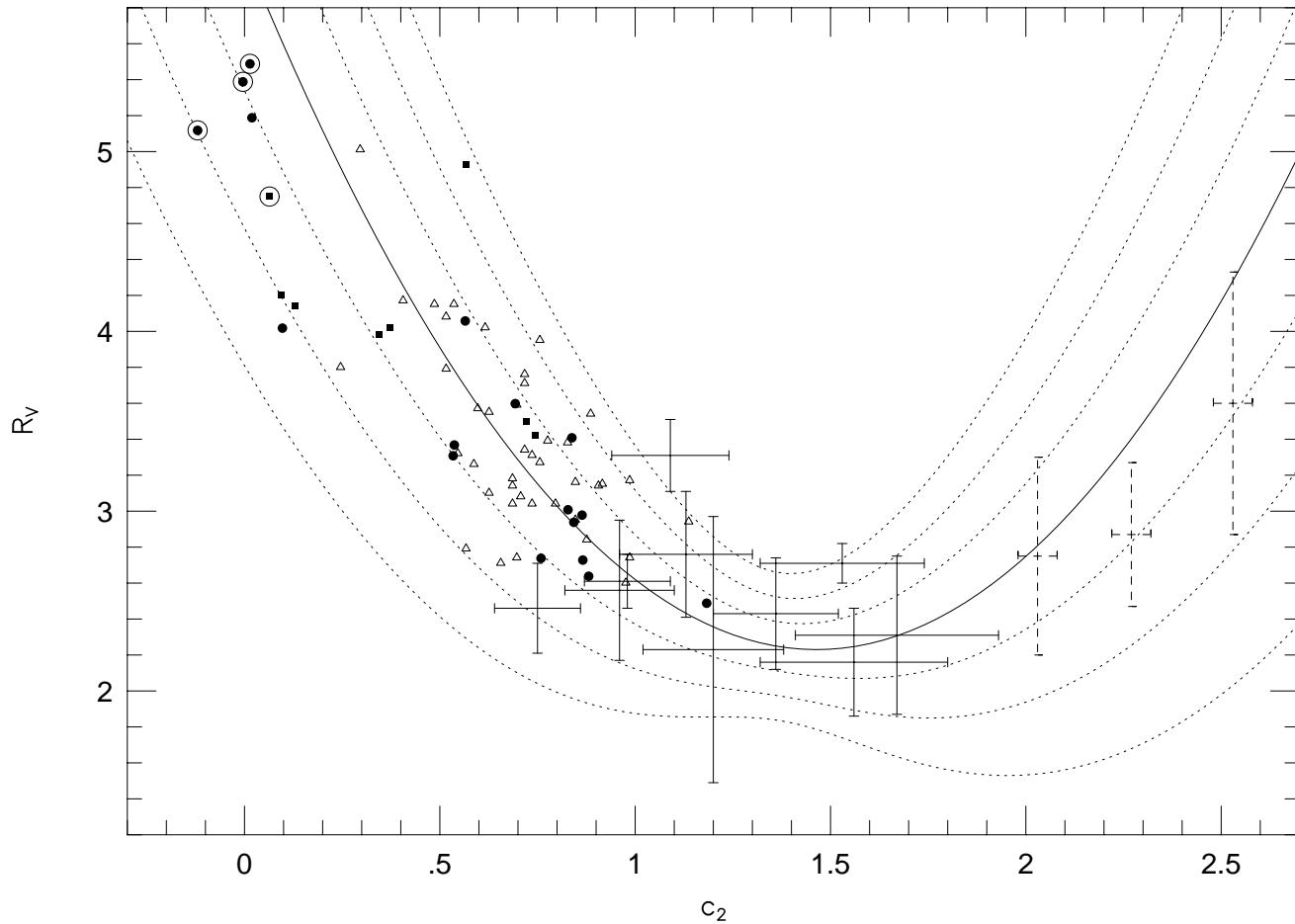
Fig. 6.— The correlation between the extinction curve parameters c_4 and c_3 (top panel), and c_4 and γ (bottom panel) as a function of c_2 (see §4.2, Figure 2, Figure 4).

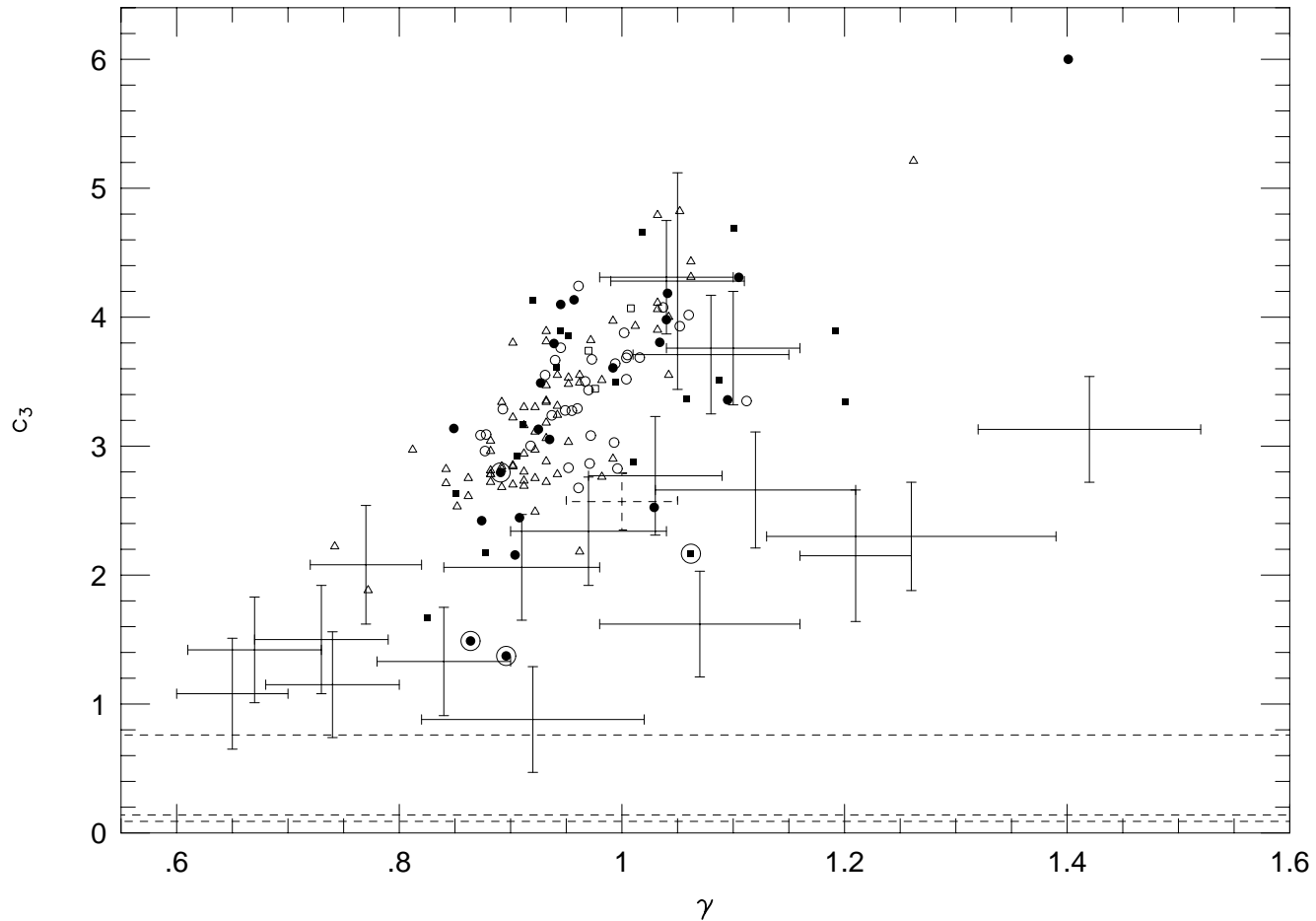
Fig. 7.— The correlation between Ly α forest flux deficit, D_A , and redshift, z . The dotted lines mark approximate 1-, 2- and 3- σ confidence regions (see §5). The circles denote Sample 2 of Zuo & Lu (1993), and the squares denote the high redshift sample of Schneider, Schmidt, & Gunn (1989a,b, 1991).

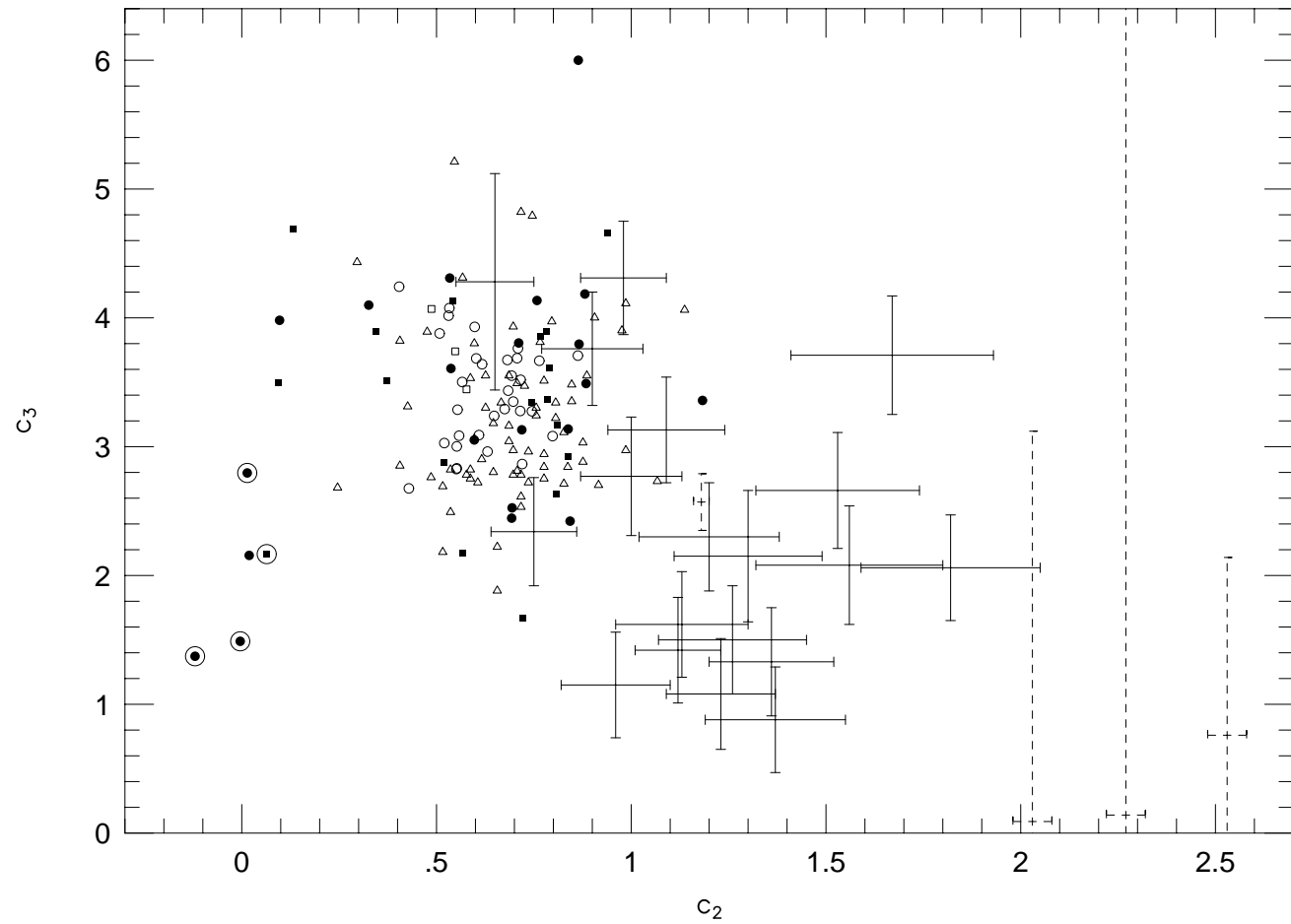
Fig. 8.— Example extinguished and absorbed spectral flux distributions (see §6). The dotted curve in each panel corresponds to an unextinguished, unabsorbed spectral flux distribution, given by $F_\nu \propto \nu^{-1}$. The top solid curve in each of the first five panels is given by $(A_V, c_2, c_3/\gamma^2, c_4, z) = (1, 0, 0, 0, 1)$. The lower two solid curves in each of these five panels is given by increasing, as marked, the value of a single of these five parameters. In the fifth (redshift) panel, we have fixed the spectral flux at long wavelengths. The solid curves in the sixth panel are typical of extinction by dust in (from top to bottom) the Orion Nebula, the diffuse ISM of our galaxy, the LMC and the SMC wing, and the SMC bar, for a variety of redshifts.

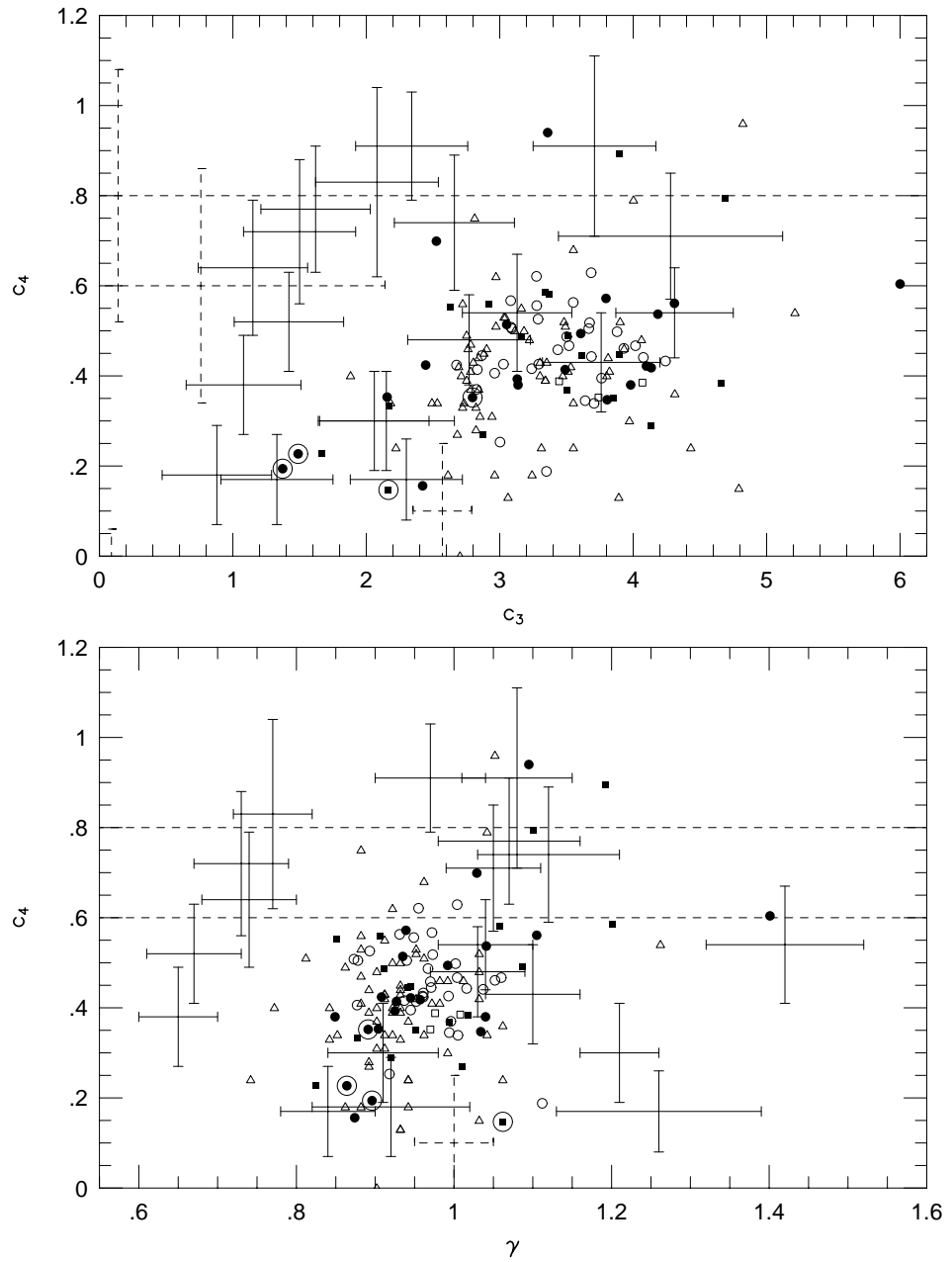


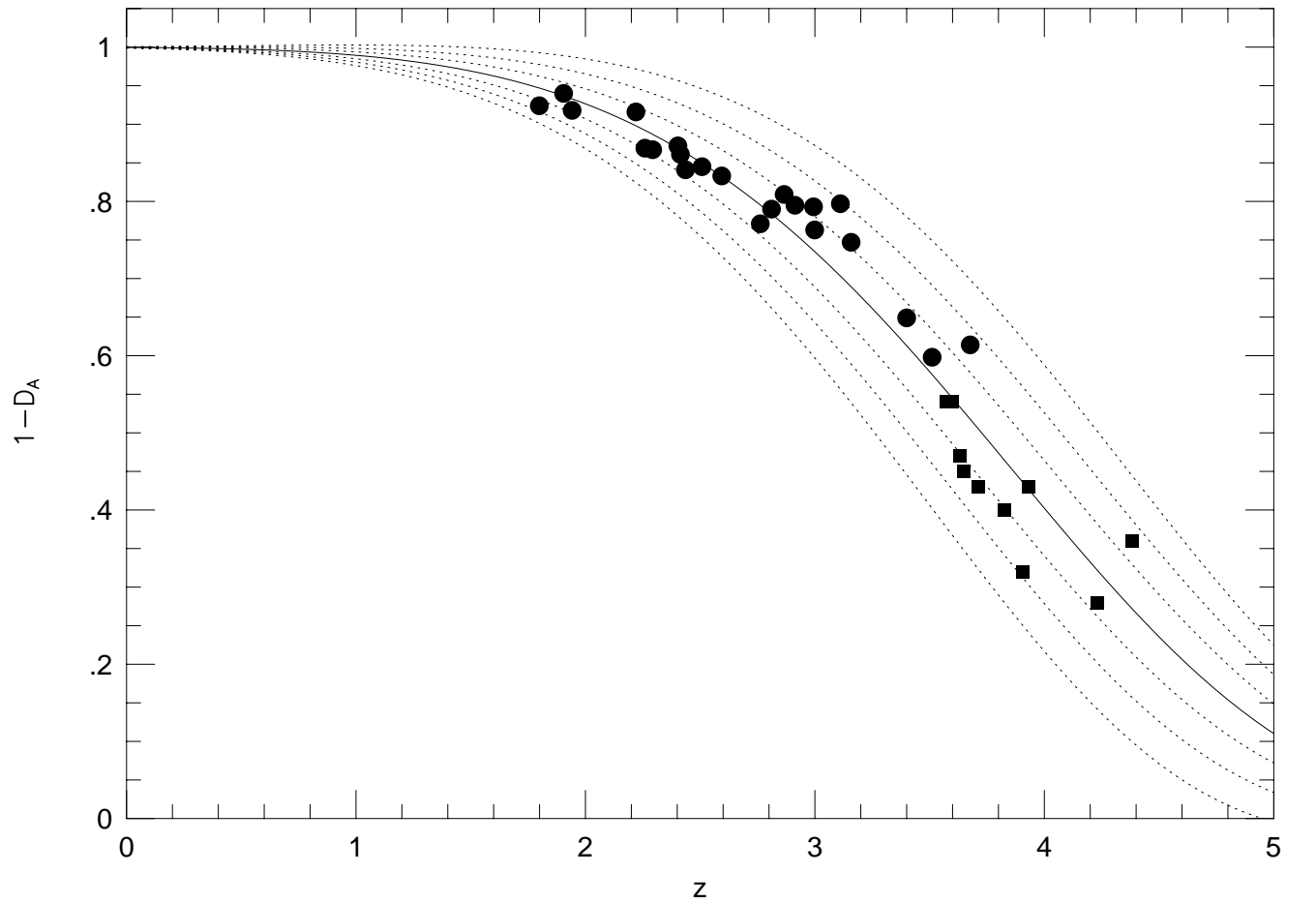












$-0V$

